Fluorescence Lifetime Imaging

13

Klaus Suhling, Liisa M. Hirvonen, James A. Levitt, Pei-Hua Chung, Carolyn Tregidgo, Dmitri A. Rusakov, Kaiyu Zheng, Simon Ameer-Beg, Simon P. Poland, Simao Coelho, Robert Henderson, and Nikola Krstajic

Contents

K. Suhling (✉) • L.M. Hirvonen • J.A. Levitt • P.-H. Chung • C. Tregidgo
Department of Physics, King's College London, London, UK
e-mail: klaus.suhling@kcl.ac.uk

D.A. Rusakov • K. Zheng
Institute of Neurology, University College London, London, UK

S. Ameer-Beg • S. Coelho
Randall Division of Cell and Molecular Biophysics, King's College London, London, UK

Richard Dimbleby Department of Cancer Research, Division of Cancer Studies, New Hunt's House, King's College London, London, UK

S.P. Poland
Division of Cancer Research and Randall Division of Cell and Molecular Biophysics, Guy's Campus, King's College London, London, UK

Richard Dimbleby Department of Cancer Research, Division of Cancer Studies, New Hunt's House, King's College London, London, UK

R. Henderson
CMOS Sensors and Systems Group, Integrated Micro and Nano Systems, School of Engineering, University of Edinburgh, Edinburgh, UK

N. Krstajic
CMOS Sensors and Systems Group, Integrated Micro and Nano Systems, School of Engineering, University of Edinburgh, Edinburgh, UK

EPSRC IRC "Hub" in Optical Molecular Sensing and Imaging, MRC Centre for Inflammation Research, Queen's Medical Research Institute, University of Edinburgh, Edinburgh, UK

A.H.-P. Ho et al. (eds.), *Handbook of Photonics for Biomedical Engineering*,
DOI 10.1007/978-94-007-5052-4_13

Abstract

Fluorescence lifetime imaging (FLIM) is a key fluorescence microscopy technique to map the environment and interaction of fluorescent probes. It can report on photophysical events that are difficult or impossible to observe by fluorescence intensity imaging, because FLIM is largely independent of the local fluorophore concentration and excitation intensity. Many FLIM applications relevant for biology concern the identification of Förster resonance energy transfer (FRET) to study protein interactions and conformational changes. In addition, FLIM has been used to image viscosity, temperature, pH, refractive index, and ion and oxygen concentrations, all at the cellular level. The basic principles and recent advances in the application of FLIM, FLIM instrumentation, molecular probe, and FLIM detector development will be discussed.

Keywords

Time-correlated single-photon counting (TCSPC) • Fluorescence microscopy • Fluorescence spectroscopy • Anisotropy • Förster resonance energy transfer (FRET) • Fluorescence anisotropy imaging (FAIM) • Time-resolved fluorescence anisotropy imaging (TR-FAIM) • Total internal reflection fluorescence (TIRF) • Fluorescence enhancement • Plasmonics

Introduction

Much of our knowledge of biological processes at the cellular and subcellular level comes from the microscope's ability to directly visualize them: optical imaging is compatible with living specimens, as light is nonionizing, nondestructive, and

minimally invasive. Fluorescence microscopy in particular combines advantages of single-molecule sensitivity, molecular specificity, subcellular resolution, and real-time data collection from live cells with negligible cytotoxicity. This allows not only the study of the structure of the sample but also the observation of dynamics and function in real time.

Among the various fluorescence microscopy methods, fluorescence lifetime imaging (FLIM) has emerged as a key technique to image the environment and interaction of specific probes in living cells [1–3]. There are several technological implementations of FLIM, but they all can report on photophysical events that are difficult or impossible to observe by fluorescence intensity imaging, because FLIM is generally independent of fluorophore concentration. The fluorescence lifetime provides an absolute measurement which, compared to fluorescence intensity, is less susceptible to artifacts arising from scatted light, photobleaching, nonuniform illumination of the sample, light path length, or excitation intensity variations.

FLIM is often used to detect Förster resonance energy transfer (FRET) to identify protein interactions or conformational changes of proteins in the life and biomedical sciences [4–10]. However, applications in diverse areas such as forensic science [11], combustion research [12, 13], luminescence lifetime mapping in diamond [14, 15], microfluidic systems [16–22], art conservation [23, 24], remote sensing [25–27], lipid order problems in physical chemistry [28], and temperature sensing [17, 21, 29, 30] have also been reported. FLIM has been carried out from the UV [31] to the visible, and it is not surprising that fluorescence lifetime-based imaging is widely used in the biomedical sciences and that this trend shows no signs of abating.

The observation of fluorescence and the use of microscopy stretches back many hundreds of years, as illustrated in Fig. 1 [32, 33]. However, the understanding of fluorescence-related phenomena and the creation of an appropriate theoretical framework to quantitatively interpret and predict fluorescence and to design a fluorescence microscope only occurred 100–150 years ago (The Nature milestone website contains a wealth of information on the history of optical microscopy: http://www.nature.com/milestones/milelight/index.html). Over the last 10 or 20 years, the field has advanced rapidly and enormously [34], mainly due to the combination of lasers and beam scanning [35], powerful computers, and also sensitive detectors and cameras [36–40] and genetic engineering [41] – the latter effort being recognized with the award of the Nobel Prize in Chemistry in 2008, for the discovery and development of the green fluorescent protein, GFP. A year later, in 2009, half of the Nobel Prize in Physics was given to the invention of the CCD sensor in 1969 [42] – a device which has also played a significant role in advancing fluorescence microscopy. The sensitivity of fluorescence detection is at the single-molecule level, and point-spread function engineering has allowed fluorescence imaging well below the spatial resolution limit given by classical optical diffraction. These "super-resolution techniques" include stimulated emission depletion (STED), structured illumination, and photoactivation and blinking localization microscopy, as reviewed recently [43–45].

While the idea of nanosecond time-resolved fluorescence measurements of samples under a microscope dates back to the 1950s [46], the emergence of FLIM as a technique for mapping fluorescence lifetimes only began in 1989. In this year, the

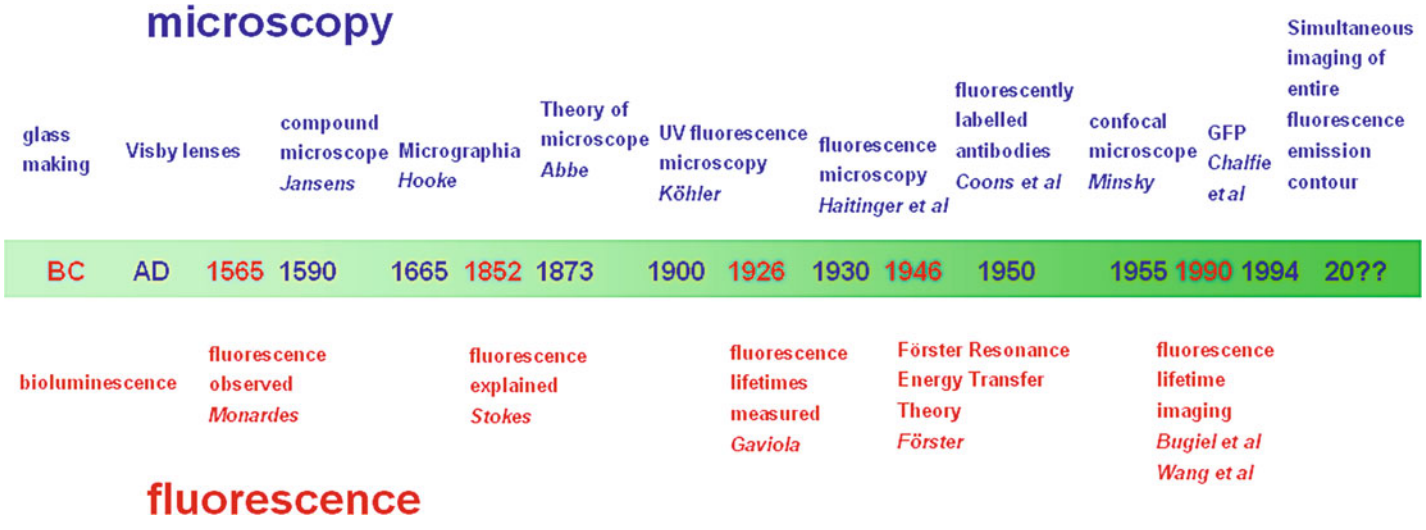

Fig. 1 A brief history of microscopy and fluorescence. The development of the microscope was essential for discovering and studying the cell, the basic and universal building block of all living organisms. The combination of microscopes with lasers, powerful computers, sensitive detectors, and cameras and the genetically encoded green fluorescent protein (*GFP*) and its variants have led to revolutionary advances in the life sciences over the last two decades

first reports were published describing a fluorescence imaging technique where the contrast in the image is provided by the fluorescence lifetime [47, 48].

Since then, the power of FLIM has increased dramatically with the extension to spectrally resolved FLIM, polarization-resolved FLIM, and rapid acquisition with single-photon sensitivity. FLIM has also been combined with other techniques, such as fluorescence correlation spectroscopy (FCS) [49–51], scanning near-field optical microscopy (SNOM) [52], atomic force microscopy (AFM) [53], fluorescence recovery after photobleaching (FRAP) [54–56], total internal reflection fluorescence (TIRF) microscopy [57, 58], STED [59, 60], coherent anti-Stokes Raman scattering (CARS) [61], and tomography [62].

The increasing popularity is facilitated by commercial availability of key enabling technology: FLIM add-on units to conventional microscopes, for wide-field, confocal, and multiphoton excitation microscopy, including data analysis software, are available from a number of specialist companies.

Fluorescence

Fluorescence as a phenomenon has been known for hundreds or even thousands of years, but the understanding and explanation of it took a long time, especially its distinction from incandescence, iridescence, or scattered light [63]. In 1852, Stokes, building on the previous work by Boyle, Newton, Brewster, Herschel, and others, explained that the emitted light was of a longer wavelength than the absorbed light [64] – an effect now known as the Stokes shift. Above all, Stokes coined the term fluorescence [64, 65]. Despite this breakthrough, some confusion remained, but it eventually faded away like fluorescence itself [66]. After some theoretical considerations regarding fluorescence lifetimes [67], the first reports on measuring nanosecond fluorescence lifetimes experimentally appeared in the mid-1920s [68].

Upon excitation into an excited state, a fluorescent molecule – a fluorophore – can return to its ground state either radiatively by emitting a fluorescence photon,

$$A^* \rightarrow A + h\nu \tag{1}$$

or non-radiatively, for example, by dissipating the excited state energy as heat [69–72]:

$$A^* \rightarrow A + \text{heat} \tag{2}$$

A^* indicates a fluorophore in its excited state and A in its ground state and $h\nu$ is a photon. The depopulation of the excited state depends on the de-excitation pathways available. Fluorescence is the radiative deactivation of the lowest vibrational energy level of the first electronically excited singlet state S_1 back to the electronic ground state S_0. The absorption and emission processes are illustrated by an energy level diagram after Jablonski [73], as shown in Fig. 2a.

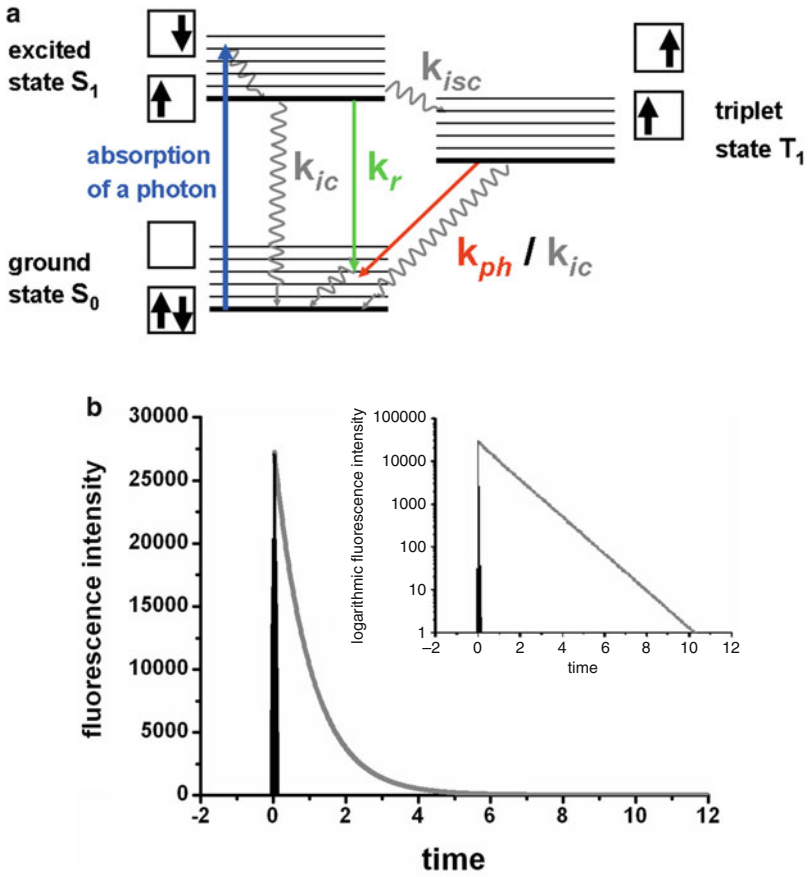

Fig. 2 (**a**) A schematic energy level diagram, after Jablonski, of a fluorescent molecule, depicting the molecular singlet and triplet electronic energy levels, each with vibrational energy levels as well as excitation and de-excitation pathways and (**b**) a schematic fluorescence decay, where the fluorescence intensity decays over time according to an exponential decay law. *Inset* is a semilogarithmic plot of the same fluorescence decay, which, convenient for easy visual inspection, appears as a *straight line*

The fluorescence lifetime τ is the average time a fluorophore remains in the electronically excited state S_1 after excitation. τ is defined as the inverse of the sum of the rate parameters for all excited state depopulation processes:

$$\tau = \frac{1}{k_r + k_{nr}} \tag{3}$$

where k_r is the radiative rate constant and the non-radiative rate constant k_{nr} is the sum of the rate constant for internal conversion, k_{ic}, and the rate constant for intersystem crossing to the triplet state, k_{isc}, so that $k_{nr} = k_{ic} + k_{isc}$. The fluorescence emission always occurs from the lowest vibrational level of S_1, a rule known as Kasha's rule [74], indicating that the fluorophore has no memory of its excitation pathway.

$\tau_0 = {k_r}^{-1}$ is the natural or radiative lifetime which is related to the fluorescence lifetime τ via the fluorescence quantum yield ϕ:

$$\phi = \frac{\tau}{\tau_0} = \frac{k_r}{k_r + k_{nr}} = \frac{1}{1 + \frac{k_{nr}}{k_r}} \tag{4}$$

The fluorescence quantum yield can be thought of as the ratio of the number of fluorescence photons emitted to the number of photons absorbed (regardless of their energy) and is less than one. And since $\phi\ \tau_0 = \tau$, τ_0 can be thought of as the longest lifetime the fluorophore can have, i.e., when $k_{nr} = 0$.

Both the fluorescence lifetime and the fluorescence quantum yield are key spectroscopic parameters, the measurement of which allows the explicit calculation of the radiative rate constant k_r and the non-radiative rate constant k_{nr}.

The radiative rate constant $k_r = {\tau_0}^{-1}$ is related to the absorption and fluorescence spectra and is a function of the refractive index of the medium surrounding the fluorophore:

$$k_r = 2.88 \times 10^{-9} n^2 \frac{\int F(\tilde{\nu}) d\tilde{\nu}}{\int F(\tilde{\nu}) \tilde{\nu}^{-3} d\tilde{\nu}} \int \frac{\varepsilon(\tilde{\nu})}{\tilde{\nu}} d\tilde{\nu} \tag{5}$$

where n is the refractive index, F is the fluorescence emission, ε is the extinction coefficient, and $\tilde{\nu}$ is the wavenumber. This equation is known as the Strickler–Berg equation [75]. Essentially, the Strickler–Berg equation is a version of the Einstein coefficients for absorption and spontaneous and stimulated emission [76, 77] but adapted for molecules with broad absorption and emission spectra, rather than atomic line spectra. A more detailed treatment taking into account the transition dipole moment, an intrinsic property of the molecule, has been devised by Toptygin et al. [78] who have also written a detailed review of the subject [79].

The time dependence of the depopulation of the excited state – the decay of the excited state – can be explained as follows. After excitation, N fluorophores will leave the excited state S_1 (see Fig. 2b) according to the following rate equation:

$$dN = (k_r + k_{nr}) N(t) dt \tag{6}$$

where t is the time, in an analogous fashion to radioactive decay. (Another analogy is that emission events are independent of one another, and both radioactive decay and photon emission are described by Poisson statistics – but there the analogy ends: radioactive decay is a nuclear process emitting photons or particles many orders of magnitude more energetic than the emission of light of energies in the range of 2–4 eV, originating from the fluorophore's electronic orbitals). Integration, using Eq. 6, and taking into account that the fluorescence intensity $F(t)$ is proportional to the excited state population $N(t)$ yields

$$F(t) = F_0 e^{-t/\tau} \tag{7}$$

where F_0 represents the fluorescence intensity at $t = 0$ and τ is the fluorescence lifetime as defined in Eq. 3. The decay of the fluorescence intensity thus follows an exponential decay law [80], schematically shown in Fig. 2b. τ is the time it takes for the fluorescence intensity to decay from its peak value to $e^{-1} \approx 37\%$ of its peak value. This applies both to repeatedly excited single molecules – where the fluorescence lifetime represents a measure of the emission probability after a certain time – and the fluorescence decay of an ensemble of fluorophores after a single excitation. Note that on a logarithmic fluorescence intensity scale, a mono-exponential decay conveniently appears as a straight line, as shown in the inset of Fig. 2b. This way of plotting the data thus aids simple visual inspection of the fluorescence decay behavior.

Fluorescence Probes

Some minerals fluoresce, and naturally occurring fluorescent dyes have been known for a long time [69, 70]. The first synthetic dye was mauve, synthesized by Perkin in Manchester in 1856 [81]. It had a low fluorescence quantum yield, but shortly afterward, in 1871, the much brighter dye fluorescein was first synthesized by von Baeyer. He was awarded the Nobel Prize in Chemistry in 1905, "in recognition of his services in the advancement of organic chemistry and the chemical industry, through his work on organic dyes and hydroaromatic compounds." This work was closely linked to color chemistry, i.e., the research into dyes for staining fabrics and other materials [81]. Often, these dyes were not fluorescent, but they did absorb light and were of major interest for the textile industry – not only in the West but also in China for staining silk, for example.

Today, fluorescence sensing and microscopy can be performed by labeling a sample with fluorescent dyes, quantum dots [82], or other nanoparticles [83, 84], including nanodiamonds [85–88] and nano-ruby [89], as reviewed recently [90]. In addition to fluorescent dyes, quantum dots and other nanoparticles have also recently found favor in cell imaging applications due to their high fluorescence quantum yield, low photobleaching susceptibility, and narrow, size-dependent emission spectra which can be excited with a single wavelength [82, 83, 91–93]. Frequently used probes in biology are genetically encoded fluorescent proteins [94] and imaging of auto-fluorescence, i.e., endogenous fluorescence from tryptophan, melanin, keratin, elastin, lipofuscin, nicotinamide adenine dinucleotide (NADH), or flavin adenine dinucleotide (FAD), or in the case of plants, chlorophyll is also increasingly used [95, 96].

FLIM Applications in the Life Sciences

Förster Resonance Energy Transfer (FRET) to Study Protein Interactions or Conformational Changes

FRET is a bimolecular fluorescence quenching process where the excited state energy of a donor fluorophore is non-radiatively transferred to a ground state acceptor molecule, as schematically illustrated in Fig. 3. The phenomenon is based

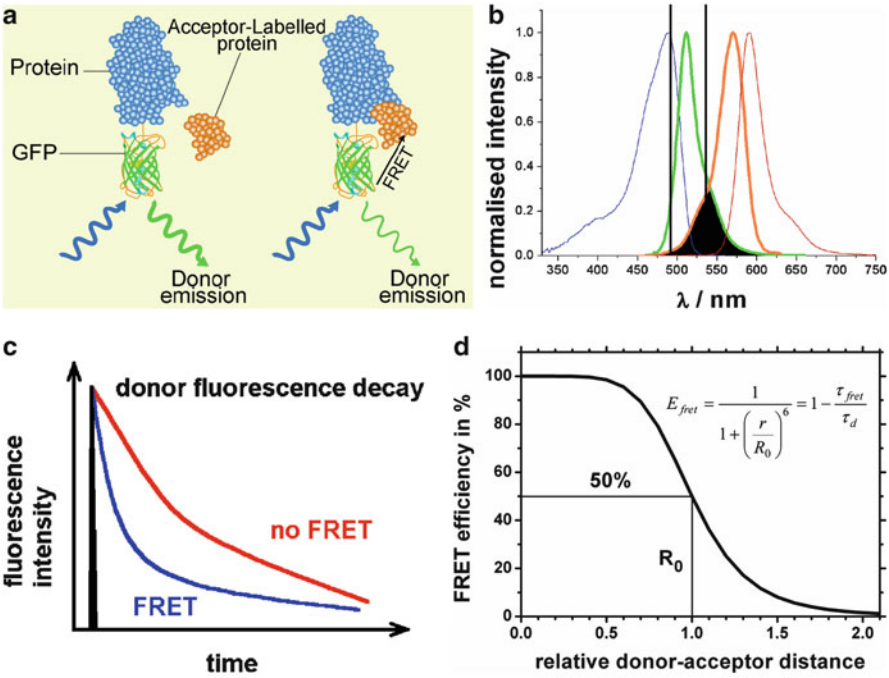

Fig. 3 Förster resonance energy transfer (*FRET*). (**a**) FRET schematic illustrating the use of this photophysical phenomenon to elucidate protein interaction between the big blue protein, labeled with GFP, and the small orange fluorophore-labeled protein. (**b**) The spectral overlap between the GFP donor emission spectrum (*green*) and the rhodamine acceptor absorption spectrum (*orange*) is indicated in *black* ("resonance"). FLIM to identify FRET can be performed by measuring the fluorescence decay of the donor in the spectral window indicated by the *black vertical bars* over the donor emission spectrum. Close proximity of donor and acceptor and favorable orientation of their transition dipole moments is also required for FRET to occur. The excited donor transfers its energy to the acceptor, whereupon the donor returns to the ground state, and the acceptor finds itself in the excited state. Note that no photons are emitted in FRET; it is a non-radiative transfer of excited state energy from the donor to the acceptor. (**c**) FRET effect on donor fluorescence decay. FRET is a quenching process, i.e., offers an additional non-radiative decay pathway in Eq. 3 and thus shortens the donor fluorescence decay. (**d**) The distance dependence of FRET. The FRET efficiency varies in proportion to r^{-6} where r is the distance between donor and acceptor, idealized as point dipoles

on a dipole–dipole coupling process and was quantitatively correctly described by Förster in 1946 [98]. FRET only occurs if the donor and acceptor fluorophores are within close proximity (typically <10 nm), and the emission spectrum of the donor and the absorption spectrum of the acceptor overlap, as indicated in Fig. 3b. In addition, the transition dipole moments of the donor and acceptor must not be perpendicular – otherwise, the transfer efficiency is zero, irrespective of the donor–acceptor distance or the spectral overlap. Finally, the multiplicity (effectively the spin of the excited electron) must be preserved by the transitions, and singlet–triplet transitions are forbidden as they require a spin flip [71]. (In this

context, note that the important singlet oxygen generation in photodynamic therapy [99], or as one of the photobleaching processes, by energy transfer from the fluorophore's triplet state occurs via Dexter-type electron exchange which does not need to conserve multiplicities.) The critical transfer distance R_0, where FRET and fluorescence emission are equally likely, can be calculated from the spectral overlap [100, 101] (Free PhotochemCAD software to calculate the R_0 for any donor–acceptor pair can be downloaded from http://photochemcad.com [99, 100]).

The FRET efficiency, *E*, varies with the inverse 6th power of the distance between donor and acceptor and is usually negligible beyond 10 nm, as shown in Fig. 3d. FRET can therefore be used as a "spectroscopic ruler" to probe inter- and intramolecular distances on the scale of the dimensions of the proteins themselves [102–104]. This is a significant advantage over co-localization studies with two fluorophores which is limited by the optical resolution of light microscopy (approximately 200 nm laterally, 500 nm axially [44] – although for single-molecule co-localization, this resolution limit is somewhat relaxed). Thus, if one type of protein is labeled with a donor and another type of protein is labeled with an acceptor, the detection of FRET yields proximity information well below the optical resolution limit that can be achieved by co-localization imaging of the two fluorophores and is interpreted as the interaction of the two proteins. In addition, FRET is also frequently used to study conformational changes within a protein [105] or cleavage of a protein or as a sensor, e.g., for Cu^{2+} ions [106] or for Ca^{2+} ions [107]. The cameleon Ca^{2+} sensor, for example, consists of cyan fluorescent protein (CFP) and yellow fluorescent protein (YFP), and FRET is induced by a conformational change upon binding of four Ca^{2+} ions, whereas in the green fluorescent protein (GFP)-based Cu^{2+} sensor, the Cu^{2+} ion itself acts as the acceptor due to its absorption in the red.

FRET, as a fluorescence quenching process, reduces the quantum yield and the fluorescence lifetime of the donor according to Eqs. 3 and 4. If the acceptor is fluorescent (which is not a necessary requirement for FRET to occur), FRET can lead to sensitized acceptor emission. To identify and quantify FRET in biological applications, the fluorescence decay of the donor can be measured in the absence and presence of the acceptor. The advantage of time-resolved over intensity-based measurements is the ability to directly distinguish between effects due to FRET or probe concentration. For example, a low donor fluorescence intensity can be caused by either a low donor concentration or efficient quenching by FRET – but only in the latter case is the fluorescence decay shortened. Indeed, FLIM is the best method to identify FRET [108, 109]. It only requires the measurement of the donor fluorescence and allows the separation of energy transfer efficiency and FRET population, independent of local concentration and stoichiometry of donor and acceptor. If the stoichiometry is not known, i.e., the sample contains both interacting and non-interacting donors, then a bi-exponential donor fluorescence decay would result. The non-interacting donors do not undergo FRET and thus emit fluorescence with the lifetime of the unquenched donor. The donors undergoing FRET exhibit a shortened fluorescence decay. The ratio of the pre-exponential factors (amplitudes) of the bi-exponential decay represents the ratio of interacting donors undergoing

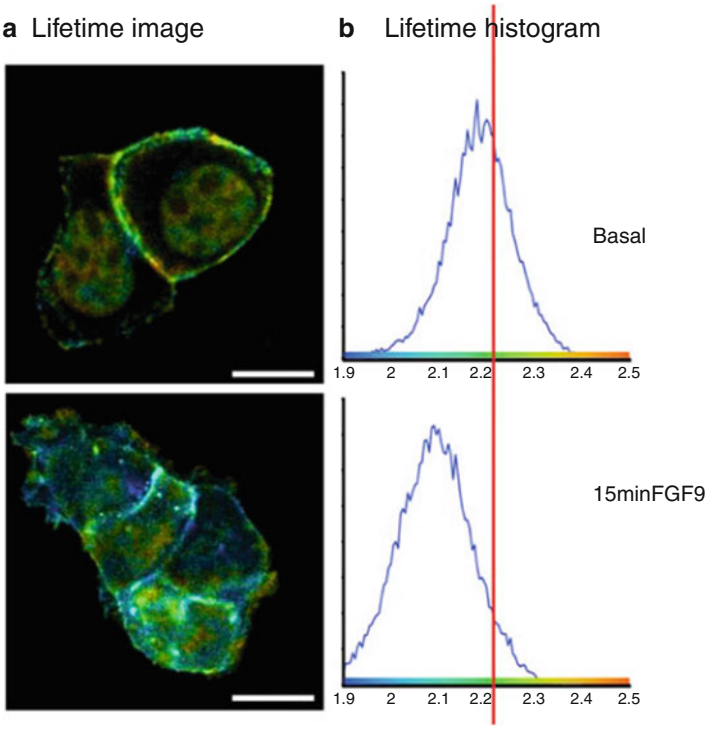

Fig. 4 An example of FRET between CFP-labeled donor proteins and RFP acceptor-labeled proteins from ref. [97]. (**a**) FLIM images. Upon 15 min stimulation with FGF9, protein interaction is induced as indicated by the reduced average fluorescence lifetime of the CFP donor. (**b**) Average fluorescence lifetime histogram of CFP donor

FRET to those not interacting [110, 111]. In practice, however, note that the complex photophysics of fluorescent proteins means they have multiexponential decays even before undergoing FRET [105, 112–115]. Moreover, due to the longer excited state lifetime, donors not undergoing FRET photobleach faster than those undergoing FRET. This latter effect may not only have to be taken into account for quantitative FRET analysis but can be also (and has been) exploited to study FRET as donor photobleaching FRET [116]. An example of FRET between CFP and RFP-labeled proteins is shown in Fig. 4 [97].

Accurate determinations of molecular separation are rarely quoted in the literature, due to uncertainty in the real value of R_0. However, the principal goal is usually the detection of FRET to infer proximity of donor and acceptor and thus interaction of the proteins they are tagged to, or conformational changes, rather than obtaining precise molecular separation.

While single-point FRET studies on cells were performed through a microscope well before the development of FLIM [117], imaging FRET can map interactions between proteins, lipids, enzymes, DNA, and RNA, as well as conformational

changes or cleavage of a protein in a two-dimensional, position-sensitive manner, so that the FRET signal provides the contrast in the image [7]. The high-resolution and optical sectioning capabilities of confocal or two-photon excitation scanning FLIM allow FRET to be mapped with great detail and protein interactions to be located accurately within different cell organelles, such as the nucleus, the cytoplasm, or the membrane.

Although most FLIM of FRET involves fluorescent proteins, this technique was already performed before the availability of fluorescent proteins. For example, intracellular fusion of endosomes or the dimerization of epidermal growth factor (EGF) or the role of the protein kinase C (PKC) family of proteins in cellular signal transduction was studied with FLIM of FRET, as reviewed previously [118]. Nowadays, fluorescent proteins can be used for genetically encoding a fluorescent label [94]. The excitation and emission spectra of the green fluorescent protein (GFP) and its derivatives span the entire visible range [119], but the photophysics of the fluorescent proteins is complex [120]. The widely used mutant enhanced GFP (F64L, S65T), for example, has at least two emitting states [112–115]. Nonetheless, FLIM of GFP and its spectral variants [119] with average fluorescence lifetimes in the 2–3 ns region has proved extremely valuable to the fluorescence microscopy community.

FLIM of Fluorescent Molecular Rotors to Map Viscosity

Fluorescent molecular rotors are fluorophores whose fluorescence quantum yield ϕ and fluorescence lifetime τ are functions of the viscosity η of their environment [121–125] where

$$\phi = z\eta^x \tag{8}$$

and

$$\tau = z'\eta^x \tag{9}$$

according to a model proposed by Förster and Hoffmann, with $x = 2/3$ [126], or later in a more general form ($0 < x \leq 1$) by Loutfy [127]. z and z' are constants, and $\phi << 1$. A key characteristic of a fluorescent molecular rotor is that, in the excited state, it can rotate one segment of its structure around a single bond and thus form a twisted state. It is this intramolecular rotation which depends strongly on the viscosity of the environment, so that the radiative de-excitation pathway of fluorescent molecular rotors competes with radiationless decay by intramolecular twisting around a single bond in the excited state. This twisting motion is slowed in viscous media. Thus, the fluorescence lifetime and fluorescence quantum yield of fluorescent molecular rotors are high in viscous microenvironments and low in non-viscous microenvironments. Fluorescent molecular rotors have been used to measure the microviscosity in polymers [127], sol–gels [128, 129], micelles [130], ionic liquids [131–133], blood

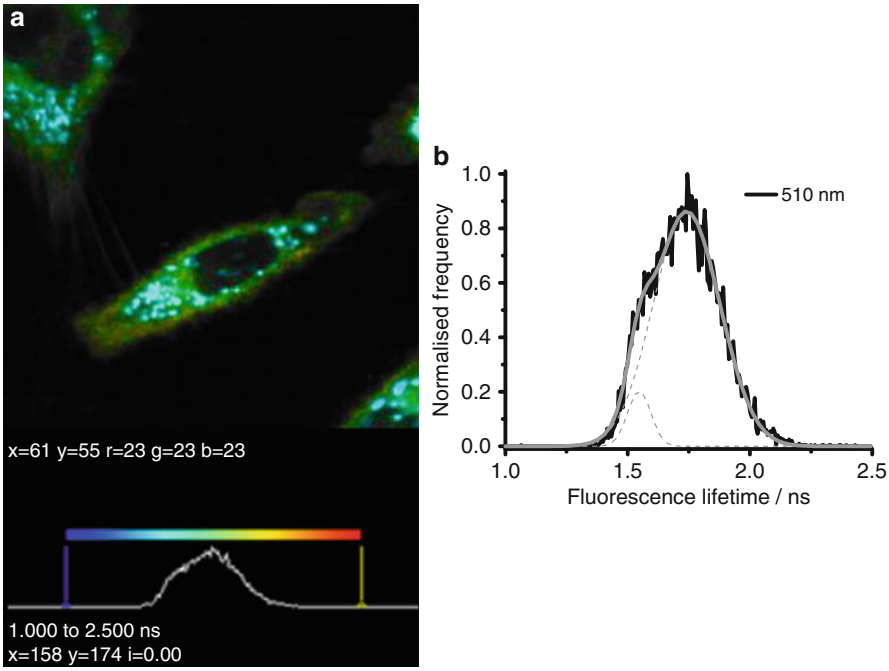

Fig. 5 HeLa cells stained with fluorescent molecular rotor Bodipy-C^{12}. (**a**) FLIM image, with lifetime indicating viscosity, and (**b**) the fluorescence lifetime histogram

plasma [134], liposomes [135, 136], and biological structures such as tubulin [137] and living cells [138–144]. The viscosity measurement can be accomplished either by ratiometric spectral measurements with a rigid reference fluorophore whose fluorescence quantum yield and lifetime are independent of viscosity [136, 140, 141, 145–148] or by fluorescence lifetime measurements [138–140, 144]. In combination with fluorescence microscopy, the use of fluorescent molecular rotors allows not only mapping the viscosity in living cells but also monitoring dynamic cellular processes in real time.

Fluorescence lifetime imaging (FLIM) of fluorescent molecular rotors has been employed to image viscosity in living cells [138–140], microbubbles [149], and *Bacillus* spores [150]. A typical example of FLIM of Bodipy-C_{12} in lipid droplets is shown in Fig. 5. The big advantage of time-resolved measurements of fluorescent molecular rotors is that the fluorescence lifetime is independent of the fluorophore concentration [136, 140, 141, 145–148]. Thus, FLIM intrinsically separates concentration and viscosity effects. There is no need to conjugate the fluorescent molecular rotors to other viscosity-independent fluorophores in order to account for variations in dye concentrations as in ratiometric intensity imaging [122]. Moreover, fluorescence lifetime measurements can detect heterogeneous viscosity environments via multiexponential fluorescence decays, potentially within a single pixel, and the lifetime calibration does not depend on the spectral sensitivity of the detection

system. Furthermore, FLIM of fluorescent molecular rotors frees the spectral region occupied by the viscosity-independent reference fluorophore for simultaneous mapping of other parameters, e.g., polarity. Thus, FLIM of suitable fluorescent molecular rotors represents a major advance in terms of straightforward calibration and rapid, real-time, and ultrasensitive detection.

FLIM to Map the Temperature

One of the latest advances in the use of FLIM is to use it in combination with special temperature-sensitive polymers to map the temperature in living cells. While FLIM of rhodamine B in methanol was used to map the temperature in a glass microchip from 10 °C to about 95 °C with a ±3 °C accuracy [17], and FLIM of Kiton red, a water-soluble rhodamine B derivative, was used to map thermal and solution transport processes in a microfluidic T-mixer [151], these dyes have a limited sensitivity to temperature. They may cover a large dynamic range from 10 °C to 100 °C, but they are not very sensitive to temperature variations around 37 °C.

Novel temperature-sensitive polymers, fluorescent polymeric thermometers, have been designed that are not very sensitive to temperature over a wide dynamic range, but rather display a large fluorescence lifetime variation near 37 °C [29]. At low temperatures, a thermo-responsive polymer assumes an extended configuration, where a water-sensitive unit can be quenched by water molecules in its vicinity. At higher temperatures, hydration is weakened and the structure shrinks, releasing water molecules and thus increasing its fluorescence quantum yield and lifetime. These sensitive fluorescent polymeric thermometers have been used in combination with TCSPC-based FLIM to map the temperature in living cells to a fraction of a degree. The resulting temperature maps illustrated thermogenesis in the mitochondria, showing that the temperature of the nucleus is about 1 °C higher than that of the cytoplasm and that this depends on the cell cycle [29].

FLIM to Map the Refractive Index

The fluorescence decay of GFP is a function of the refractive index of its environment [112, 152, 153]. The reason for this is that the radiative rate constant, k_r (see Eq. 5), is a function of the refractive index, n [79]. This effect, expressed empirically as an n^2 dependence of the radiative rate constant in the Strickler–Berg formula, has been predicted theoretically and demonstrated experimentally for fluorescent dyes, lanthanides, quantum dots, and nanodiamonds over the years, varying the refractive index by solvent composition or pressure, including supersonic jet spectroscopy in vacuum [112]. In the particular case of GFP, the non-radiative rate constant seems to be insensitive of the environment, as the GFP fluorophore is tightly bound inside its barrel, protected from solvent effects, oxygen quenching, and other diffusion-controlled collisional quenching effects – influences of fluorescent dyes in solution are generally subjected to. The range over which the GFP decay senses the refractive

index can be large, up to hundreds of nm, depending on the experimental details [153]. It plays a role in TIRF FLIM, since GFP in close proximity to a glass–water interface has a lower average decay time than far away from the interface [153] and has been used to study GFP infiltration into the nanochannels of mesoporous silica particles [154].

In combination with FLIM, this effect has been exploited to show that GFP-tagged proteins have a faster decay in the cell membrane compared to the cytoplasm, owing to the membrane's higher refractive index [155]. In another study, the fluorescence decays of cytoplasmic GFP and also of tdTomato, a red fluorescent protein, were mapped during mitosis, showing that the average GFP and tdTomato lifetimes remained constant during mitosis but rapidly shortened at the final stage of cell division [156]. The interpretation of this observation put forward was that the concentration of proteins – which have a high refractive index – in the cell changes during the cell cycle. Reports that the average GFP fluorescence lifetime of maltreated cells changes may be related to this effect too [157].

FLIM of Metal-Modified Fluorescence

While fluorescence lifetime changes due to the effect the refractive index has on the radiative rate constant k_r are modest [79], metal-induced fluorescence lifetime modifications can be much stronger [158]. In the presence of a metal, the excited state molecular dipole can couple with surface plasmons, i.e., collective electron oscillations, in the metal creating additional radiative k^*_r and non-radiative decay channels k^*_{nr} [158–160].

In such a case, Eq. 3 for the fluorescence lifetime has to be modified and the metal-modified fluorescence lifetime is then given by

$$\tau = \frac{1}{k_r^* + k_r + k_{nr} + k_{nr}^*} \tag{10}$$

with the corresponding modified Eq. 4 for the metal-modified quantum yield

$$\phi = \frac{k_{nr} + k_{nr}^*}{k_r^* + k_r + k_{nr} + k_{nr}^*} \tag{11}$$

The additional deactivation pathways are strongly dependent on the separation between the emitting fluorophore and the metal; hence, Eqs. 10 and 11 predict that as k^*_r increases near a metal surface, the fluorescence quantum yield increases while the fluorescence lifetime decreases. However, within 5–10 nm of the metal, the additional non-radiative channel k^*_{nr} dominates, leading to a strong quenching of the fluorescence, reducing the quantum yield as well.

This metal-enhanced fluorescence effect was exploited to study a multilayered polyelectrolyte film incorporating aluminum tetrasulfonated phthalocyanine (AlPcTS), a dye also used as a photosensitizer, and gold nanoparticles. The authors

found that fluorescence enhancement can be tuned by the number of polyelectrolyte layers separating AlPcTS and the gold nanoparticles [161].

Moreover, FLIM of metal-enhanced fluorescence can provide increased axial specificity in fluorescence microscopy. After demonstration of the fluorescence enhancement effect on fluorescently labeled beads on a gold film, a calibration system that closely mimics a cell imaging geometry, Cade et al. studied mammary adenocarcinoma cells expressing GFP-labeled membrane proteins grown on a 30 nm gold film [162]. FLIM images show a significantly reduced GFP lifetime in the membrane near the gold film, but the GFP lifetime was unmodified in parts of the cell further above the gold film. Thus, the GFP fluorescence lifetime yields information about the proximity of the GFP to the gold film within the confocal volume without resorting to techniques such as TIRF, SNOM [163], or 4Pi microscopy [43, 44]. This was then exploited to study receptor internalization, i.e., protein redistribution, during receptor-mediated endocytosis [162], a technique which has recently been improved by using a bespoke plasmonic nanostructure-coated glass substrate [164]. A similar approach was used to obtain axial distances in tilted microtubules up to 100 nm above a metal surface [165].

FLIM to Map Glucose

Among the reporters for fluorescence-based glucose sensing, the glucose/galactose binding protein (GBP) undergoes a large conformational change upon glucose binding [166]. This can either be detected with FRET or by labeling with an environmentally sensitive fluorophore such as Badan near its glucose binding site. The latter path was chosen, and it was found that glucose binding resulted in a large increase of fluorescence quantum yield and lifetime [167]. Agarose beads with bound GBP–Badan were imaged by FLIM, and the addition of glucose resulted in a Badan lifetime shift from 2.2 ns at zero glucose to around 2.7 ns in a 100 mM saturated glucose solution [168].

The authors point out that the fluorescence lifetime is a particularly useful parameter to perform glucose sensing, since it is relatively independent of light scattering in tissue, signal amplitude fluctuations, and fluorophore concentration. The fluorescence lifetime is thus a good alternative to electrochemistry or glucose oxidase methods, which have limited accuracy and impaired responses in vivo, possibly due to interfering electroactive substances in the tissues, coating of the sensor by protein and cells, and changes in blood flow that alter oxygen access [168].

FLIM to Map Ion Concentrations

Ions play a major role in living cells and organisms, and mapping and measuring ion concentrations and dynamically observing changes and fluctuations are of great interest to cell biologists and physiologists [169]. The most important ions are Ca^{2+}, Na^{+}, K^{+}, and Cl^{-}, and a number of different strategies employing

fluorescence-based ion sensing exist. Mapping ion concentrations via the fluorescence lifetime with FLIM in principle offers the advantage of being independent of the fluorophore concentration. FLIM is also unaffected by variations of illumination intensity or photobleaching – provided the probes do not aggregate and the photoproducts do not fluoresce. However, in practice, multiexponential decays and undesirable photoproducts may hamper applications of some probes [170].

For example, instead of using intensity-based imaging of ratiometric probes, the fluorescence lifetime of the Ca^{2+} sensor Quin-2 [170, 171] has been used to image Ca^{2+} concentration in cells. Quin-2, excited at 340 nm, unfortunately forms a photoproduct with a different Ca^{2+} affinity [170], but Calcium Crimson [172], Calcium Green [173], and Fluo-3 [174] do not suffer from this problem, although the lifetime change upon Ca^{2+} binding is not as large as in the case of Quin-2.

The fluorescence lifetime of the Cl^- sensing dye *N*-(ethoxycarbonylmethyl)-6-methoxy-quinolinium bromide (MQAE) has been used to probe Cl^- concentrations in cockroach salivary acinar cells [175] and in mammalian olfactory sensory neurons [176, 177]. The dye's sensitivity to Cl^- is due to collisional quenching which obeys Stern–Volmer kinetics [67] and can be mapped with FLIM.

A Cu^{2+} sensor based on FRET between GFP as the donor and Cu^{2+} has been reported [106] and employed for mapping Cu^{2+} ion uptake and release in plant cells via FLIM [178]. K^+ and Na^+ probes are important for hypertension measurements in blood, and lifetime measurements for this purpose have been reported [179], albeit without imaging. A range of Mg^{2+} lifetime probes have also been tested, but again without imaging [180].

FLIM to Map the pH

Other examples of FLIM are mapping the pH – or H^+ ion concentration – in single cells [181–183] and skin [184, 185]. Here the pH sensor 2,7-bis-(2-carboxyethyl)-5-(and-6) carboxyfluorescein (BCECF) was used to image pH in the skin stratum corneum. The authors used two-photon excitation FLIM to nondestructively obtain pH maps at various depths, which is difficult to achieve by nonoptical methods. Moreover, as the authors point out, intensity-based fluorescence imaging of the pH probe could not have been used for their study as the observation of a variation in fluorescence intensity could be ascribed to either a change in pH or a variation of the local probe concentration.

FLIM of GFP excited at 405 nm where the extinction coefficient is very low and the neutral fluorophore is predominantly excited has been reported to be pH sensitive. The average lifetime increases as the pH increases, and this has been applied to measure the pH between 4.5 and 7.5 in HeLa cells [186]. The same team has repeated this feat without GFP, using autofluorescence of cells, namely, the nicotinamide adenine dinucleotide (NADH) fluorescence lifetime, upon excitation at 370 nm. The authors found that the NADH lifetime decreases as pH increases [187].

FLIM to Map Oxygen

Oxygen concentrations, or partial pressures, can be sensed using long-lived ruthenium-based sensors [188–191]. TCSPC-based FLIM has been used to detect pericellular oxygen concentrations around isolated viable chondrocytes seeded in three-dimensional agarose gel, revealing a subpopulation of cells with spatial oxygen gradients [190]. Furthermore, FLIM of a long-lived ruthenium-based oxygen sensor with an unquenched decay time of 760 ns has been used to map oxygen concentrations in macrophages [191]. Lifetime measurements are particularly advantageous, since intensity-based fluorescence imaging of oxygen in cells would require a calibration of the intensity of the probe unquenched by oxygen as well as knowing its concentration in the cell. This is not practically possible. Temporal focusing for two-photon wide-field excitation with a frequency-domain FLIM system has recently been reported to image ruthenium lifetimes in cells [192]. This approach allows rapid optical sectioning with wide-field excitation and camera detection.

FLIM of Autofluorescence of Tissue, Eyes, and Teeth

FLIM of autofluorescence is an area that has recently expanded rapidly [2, 193]. The advantage of this approach is that no specific labeling is needed, as the fluorescence signal is provided, for example, by endogenous fluorophores such as nicotinamide adenine dinucleotide (NADH) or flavin adenine dinucleotide (FAD) [194]. The fluorescence lifetimes provide a readout of the metabolic state of the samples under investigation. Over 20 years ago, it was demonstrated that FLIM can map free and protein-bound NADH [195] and has been known for even longer that the redox state of the mitochondrion can be monitored by NADH fluorescence, as reviewed by the discoverer of this effect, Britton Chance [196]. Breast cancer cells have been studied by FLIM of NADH [197–201], and this approach has been extended to include FAD [202, 203]. Autofluorescence of cardiac myocytes has been studied with FLIM [204, 205], and it has been shown that FLIM of autofluorescence can distinguish necrosis from apoptosis [206]. Employing phasor analysis of the FLIM data, bacteria and cells have also recently been studied with this method in real time [207–209].

FLIM of autofluorescence has potential as a label-free clinical diagnostic tool for in vivo optical biopsies, in particular for skin [210–215]. These three-dimensional optical biopsies do not require any removal of tissue samples or any other mechanical or chemical treatment. It provides information on morphology and metabolism at a subcellular level, and it has been shown that FLIM of skin autofluorescence can distinguish basal cell carcinoma from the surrounding skin [210] and benign melanocytic nevi from malignant melanocytic lesions [216]. A combination of FLIM of autofluorescence with coherent anti-Stokes Raman spectroscopy (CARS) could add information about chemical vibrational fingerprint and also lipid and water content to the optical biopsy [217]. Apart from early detection of skin diseases, these approaches could also be used to monitor the progression of wound healing and the effect of cosmetics on the skin [218].

Another application with direct clinical relevance is autofluorescence FLIM of the eye. The autofluorescence decay of the retina is multiexponential, and a scatter plot of short versus long autofluorescence lifetimes appears to be different for healthy retinas and retinas at the onset of age-related macular degeneration (AMD) [219, 220]. This approach may offer the opportunity for early detection and diagnosis of this debilitating eye disease.

Moreover, the autofluorescence of teeth has also been studied with FLIM [221–223], and efforts are underway to use FLIM, possibly combined with endoscopy, for clinical diagnostics [224, 225] and brain tumor image-guided surgery [226].

Plant autofluorescence, i.e., FLIM of chlorophyll in algae, has recently been used to study cadmium toxicity. After careful calibration of the chlorophyll fluorescence under different excitation conditions, it was found that cadmium exposures appear to lengthen the average chlorophyll fluorescence decay, possibly due to disruption of the electron transport system in photosynthesis [227]. The authors point out that the characteristics of the chlorophyll fluorescence decay could serve as a noninvasive indicator of cadmium toxicity in algae.

Finally, the supramolecular organization of DNA has been probed with FLIM [228–231]; amyloid beta plaques, relevant for, e.g., Alzheimer's disease, have been investigated with FLIM [232–234]; and even hematoxylin and eosin staining, a standard technique in histology, has been subjected to FLIM in a quest for more information than from the hematoxylin and eosin intensity images alone [201, 235].

FLIM Implementations

The nanosecond time resolution required to measure fluorescence lifetimes can be obtained either in the time domain by exciting the sample with a short optical pulse and directly observing the decay of the fluorescence intensity or in the frequency domain by modulating the excitation source and/or the detector gain [236].

Scanning FLIM: Confocal or multiphoton excitation scanning microscopes provide inherent optical sectioning, and here FLIM is essentially a series of single-channel fluorescence lifetime measurements where the fluorescence decay is acquired in each pixel of the image by time-correlated single-photon counting (TCSPC) [47, 50, 152, 237], gated photon counting [238, 239], streak cameras [240–242], or phase modulation [243–245]. TCSPC is the gold standard for fluorescence lifetime measurements [246, 247]. TCSPC-based FLIM has the best signal-to-noise ratio of any FLIM technique [248–250], single-photon sensitivity, clearly defined Poisson statistics, and a wide dynamic range and offers an easy visualization of fluorescence decays. A schematic TCSPC-based scanning FLIM setup is shown in Fig. 6.

Using dedicated electronics, in TCSPC, the arrival time of single fluorescence photons is recorded to picosecond accuracy after exciting the sample with a short laser pulse: a constant fraction discriminator (CFD) for the shaping of the detector pulse to enable precise timing, a time to amplitude converter (TAC) for the timing,

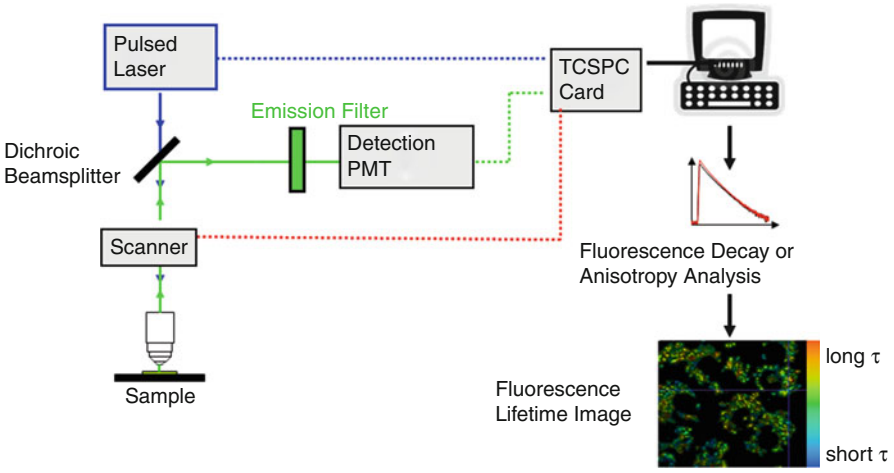

Fig. 6 A schematic TCSPC-based scanning FLIM setup

and an analogue-to-digital converter (ADC) and multichannel analyzer (MCA) to allocate the count to its time channel. By exciting the sample at MHz rates, i.e., millions of times per second, and recording the arrival time of many fluorescence photons, a probability distribution histogram of fluorescence photon arrival times is built up in the MCA. This is, in fact, the fluorescence decay curve [246, 247, 251].

As excitation sources, tunable dye lasers can be used, but their small tuning range of ≈100 nm and cumbersome operation are a disadvantage. Tunable mode-locked solid-state lasers such as Ti:sapphire lasers are much more user-friendly and provide picosecond or femtosecond pulses over a wider tuning range (≈680–1,080 nm). They can have an average power up to several watts and a fixed repetition rate of about 80 MHz which corresponds to 12.5 ns between pulses (round-trip time of a pulse in the laser cavity) and are often used as excitation sources for TCSPC FLIM, in particular for two-photon excitation FLIM but also frequency doubled for single-photon FLIM (≈340–540 nm). The repetition rate can be reduced by pulse pickers or cavity dumpers, which employ acousto-optical devices to select only a specified fraction of the pulses in the pulse train, or by long cavity lasers [252]. Small and inexpensive low average power (~1 mW) picosecond diode lasers at fixed wavelengths with variable repetition rates have also been employed for TCSPC FLIM [153], and their variable repetition rate is particularly suited to measuring long fluorescence decays, e.g., those of quantum dots.

A relatively recent innovative development is the use of a photonic crystal fiber as a tunable supercontinuum excitation source for FLIM [253]. Ti:sapphire laser pulses at 790 nm were coupled into a 30 cm long, 2 μm diameter, microstructured photonic crystal fiber to produce a continuum of pulses from 435 to 1,150 nm. Appropriate spectral selection allowed the excitation of GFP and autofluorescence in confocal TCSPC and wide-field time-gated FLIM. The ease and simplicity with which the

tunability is achieved over such a large range is a distinct advantage of this approach. Supercontinuum sources are now commercially available and have been used for FLIM [223, 234, 254].

Photomultipliers in the photon counting mode are the most frequently used detectors. They are small, reliable, and relatively inexpensive but can be damaged by excessive signals and have a transit time spread of ≈150 ps which is longer than a typical optical excitation pulse. Microchannel plates (MCPs) have the best time resolution, down to ≈20 ps, but they are expensive and can also be easily damaged by too high a light level. An alternative detector is a single-photon avalanche diode (SPAD, biased above the diode breakdown voltage) which is inexpensive, has a high detection sensitivity (quantum efficiency), and is not damaged by high light levels, but only has a small active area, a few tens or hundreds of μm^2 [36, 39, 255]. Devices with a transit time spread of only ≈40 ps have recently become available, but the light has to be focused very well onto its 20 μm diameter active area (for comparison, a typical photomultiplier or MCP cathode diameter is around 10 mm). The best detectors currently available are hybrid detectors which consist of a photocathode in front of an avalanche photodiode (APD, biased below the diode breakdown voltage). The single photoelectrons liberated by photons at the photocathode are accelerated across a high voltage (8 kV) into the APD. They have a GaAsP photocathode with a high quantum efficiency of 50% around 500 nm and a large active area, are free of afterpulsing, and cost less than a MCP. However, they can have a high dark count rate of 1,000 counts/s [256, 257]. The timing characteristics of each type of these detectors are illustrated in Fig. 7.

TCSPC is a mature and reliable digital technique based on whether a photon is detected or not [258]. The ease of reproducibility of measurements is due to the unique combination of advantages such as single-photon sensitivity, a high temporal resolution (picoseconds), linear recording characteristics independent of excitation intensity fluctuations, detector gain variations and photobleaching, well-defined Poisson statistics, wide dynamic range (in practice up to 5 orders of magnitude), and an excellent signal-to-noise ratio. It is based on timing at most one photon after an excitation pulse, so the fluorescence count rate is usually one or two orders of magnitude lower than the excitation rate. In practice, the fluorescence photon triggers the detection electronics, rather than the high repetition rate laser. This reverse mode operation minimizes the acquisition time [259].

A similar but rather faster approach is to bin all incoming photons within preset time windows after excitation [238, 239]. This time-binning method is significantly faster than TCSPC because it is not necessary to reduce the fluorescence signal to the level of single-photon timing. However, it is less accurate than TCSPC, and its time resolution is lower. The use of two-photon excitation streak-camera-based line-scanning FLIM has also been reported [240]. This technique in principle allows rapid data acquisition even for a large number of pixels, and streak cameras are the fastest detectors available.

Frequency-domain fluorescence lifetime measurements have also been combined with confocal/multiphoton laser scanning microscopy [243–245]. The advantage here is that this approach is fast and can be inexpensive [243].

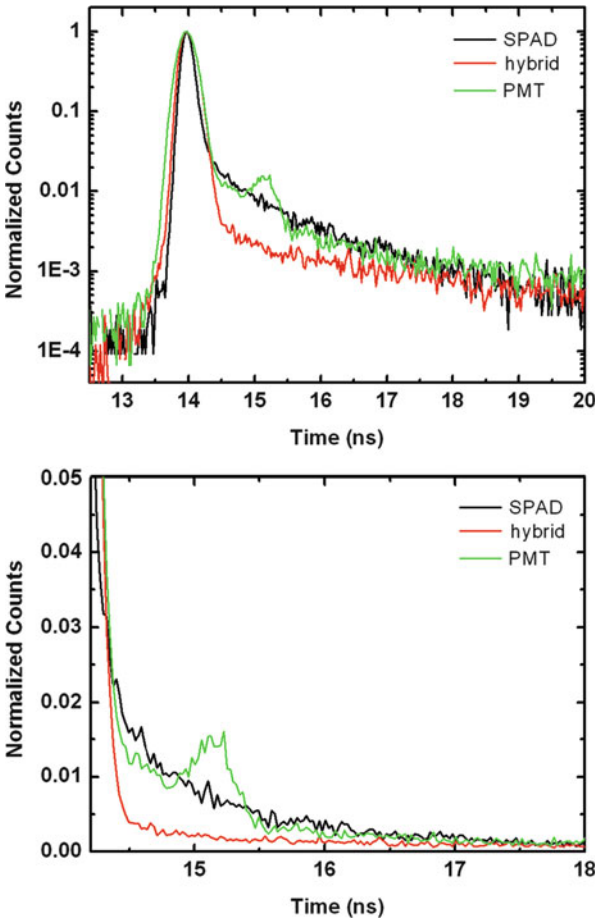

Fig. 7 A comparison of the instrumental response function of photomultiplier, SPAD, and hybrid detector to illustrate their timing characteristics. The secondary pulse of the photomultiplier and the charge carrier diffusion tail in the SPAD are evident, as is their absence in the hybrid detector. The full width at half maximum is very similar for the SPAD and hybrid detector, whereas for the photomultiplier, it is larger than either of them

Wide-Field FLIM: In the time domain, a fluorescence decay curve can be directly acquired after excitation of the sample, usually using a sampling technique [260–263]. After exciting the sample with an ultrashort laser pulse, time-gated snapshots of the fluorescence emission are taken at various nanosecond delays using high-speed gated image intensified cameras. These stroboscopic approaches are fast, since all the pixels are acquired in parallel – a 100 Hz FLIM frame rate has been reported using two time gates and an optical delay [264] – but they lack single-photon sensitivity, precision, and accuracy and are of limited suitability for single-molecule tracking, and their temporal resolution is limited to ≈80 ps [265]. However, the development of a segmented gated image intensified camera allows the simultaneous acquisition of four time gates after one excitation pulse and minimizes photon loss [266]. Directly gated CCD cameras have also been developed [267, 268], but their time resolution is lower than gated image intensified cameras and is more suited to imaging long lifetime probes.

In frequency-domain wide-field FLIM, a sinusoidally modulated excitation beam and detector may be used to measure the phase shift and demodulation of fluorescence signals with respect to their excitation signals using modulated intensified cameras [269–273]. With this approach, a fluorescence lifetime may be calculated from both the phase shift and demodulation (at several modulation frequencies if necessary, e.g., for multiexponential fluorescence decays) [274]. For a simple monoexponential fluorescence decay, both calculations should yield the same value. For more complex decays, e.g., in the case of cyan fluorescent protein, the phase shift lifetime is shorter than the demodulation lifetime [270].

The big advantage of wide-field FLIM is that it does not require scanning and has the potential for rapid refresh rates due to the parallel acquisition of all pixels. This is important for real-time FLIM [275] for biomedical applications, e.g., endoscopy [224, 225, 276, 277], and for observation of dynamic events in real time.

There is a lively debate as to the relative merits of time- or frequency-domain approaches to FLIM, as recently reviewed [236]. In theory, the two approaches are related by a Fourier transformation and, using a hybrid TCSPC and multifrequency phase fluorometer, have experimentally been demonstrated to be equivalent [278]. To nonspecialists, the easy visualization of fluorescence decays in the time domain may be an advantage over the frequency domain, where the analysis of complex fluorescence decay profiles, such as stretched exponential decay profiles, is less tractable [279]. However, for some applications, the frequency-domain instrumentation is considered easier to implement since ultrashort pulsed laser sources are not required, especially for longer lifetimes – although practitioners are increasingly using mode-locked lasers for frequency-domain measurements, particularly in multiphoton microscopes [184, 185]. Frequency-domain techniques are slightly more photon efficient than time-gating techniques (but this does not necessarily translate into more accurate fluorescence lifetimes) and require no temporal deconvolution of the instrumental response and the fluorescence decay. The signal-to-noise ratio is higher for TCSPC than for frequency-domain measurements, particularly at low intensities, but TCSPC saturates at high fluorescence intensities [249, 250].

One potential pitfall of the time-domain approach is that there should be sufficient time ($\approx 5\tau$) between excitation pulses for the sample fluorescence to completely decay in order to obtain accurate fluorescence lifetime values. In practice, this implies using mode-locked lasers with pulse pickers and cavity dumpers, lower repetition rate pulsed diode lasers [153, 280–282], long cavity lasers [252], or appropriate fitting procedures to take residual fluorescence into account [283]. This is not an issue for the frequency-domain approach. However, frequency-domain FLIM can suffer from aliasing and photobleaching-induced artifacts [284, 285] and a limited dynamic range [286].

FLIM techniques continue to be improved, particularly by the reduction of acquisition times [239]. The relative merits of the various FLIM implementations are summarized in refs [32, 118], and the choice of system depends on the samples to be studied and the practitioner's preference for fast data acquisition and high temporal or spatial resolution. In addition, some microscopy techniques such as TIRF, supercritical angle fluorescence, or selective plane illumination are difficult or

impossible to implement with scanning, and image acquisition has to be performed in wide-field mode with a camera. In combination with FLIM, this has until recently meant that gated or frequency-domain camera-based FLIM had to be used, but wide-field TCSPC methods have been improved to take advantage of the high signal-to-noise ratio available by using this type of FLIM [36, 255].

Spectrally Resolved FLIM

Spectrally resolved FLIM allows the fluorescence lifetime and spectra of two or more fluorophores to be observed simultaneously. This is advantageous in FRET studies, where the donor fluorescence lifetime can be monitored in one spectral channel and the acceptor fluorescence in another. A shortening of the average fluorescence lifetime of the donor cyan fluorescent protein (CFP) due to FRET to the acceptor yellow fluorescent protein (YFP), both linked by a short amino acid chain, was accompanied by an initial rise of the YFP fluorescence lifetime in the acceptor channel (acceptor ingrowth) due to sensitized emission [287]. Other spectrally resolved FLIM applications concern studies where the fluorescence lifetime of fluorophores emitting in different spectral regions is monitored simultaneously [244], including single-molecule studies [288]. The spectral resolution in these cases is really a spectral separation, namely, between the two spectral regions of fluorescence emission. However, true spectrally resolved FLIM with 10 nm bandwidth over a wide spectral range has been reported, both in the frequency domain [289] and the time domain (using a 16-anode photomultiplier) [290], allowing sophisticated analysis of multiple fluorophores sensing multiple biophysical parameters, FRET, and possibly multiple donor–acceptor pairs.

Polarization-Resolved FLIM

In order to maximize the information available from a limited fluorescence photon budget, it is advantageous to record multiple fluorescence parameters – such as lifetime, spectrum, and polarization – in a single imaging experiment [291]. Fluorescence is polarized due to the existence of a transition dipole moment of the fluorophore and thus the electric dipole characteristics of the emission. Polarization-resolved fluorescence measurements have been performed since the 1920s [98], and the use of fluorescence anisotropy in imaging and for single-molecule work has been reviewed recently [291–297]. When using fluorescence as a probe, polarization-resolved measurements can yield information on the properties of a sample that cannot be extracted by intensity and lifetime methods alone [298, 299].

In a polarization-resolved fluorescence microscopy experiment, a fluorescently labeled sample is excited using linearly polarized light, and the time-resolved fluorescence intensity is measured at polarizations parallel and perpendicular to that of the exciting light. The fluorescence decay parallel to the polarization of the excitation, $F_{||}$, is given by

$$F_{||}(t) = \frac{1}{3}F_0\exp\left(-\frac{t}{\tau}\right)\cdot\left[1 + zr_0\exp\left(-\frac{t}{\theta}\right)\right] \tag{12}$$

and the fluorescence decay perpendicular to the polarization of the excitation, $F_{\perp}$, is

$$F_{\perp}(t) = \frac{1}{3}F_0\exp\left(-\frac{t}{\tau}\right)\cdot\left[1 - r_0\exp\left(-\frac{t}{\theta}\right)\right] \tag{13}$$

where r_0 is the initial anisotropy and θ the rotational correlation time [69, 70]. The difference between the parallel and perpendicular fluorescence signals is due to depolarization of the fluorescence. The fluorescence anisotropy r is then defined as

$$r(t) = \frac{F_{||}(t) - GF_{\perp}(t)}{F_{||}(t) + zGF_{\perp}(t)} \tag{14}$$

where $F_{||}(t)$ and $F\perp(t)$ are the fluorescence intensity decays parallel and perpendicular to the polarization of the exciting light. The value of z depends on the NA of the microscope objective, where $1 \leq z \leq 2$ ($z \approx 1$ for a high NA objective, $z = 2$ for a collimated beam) [300–307]. Although a rigorous treatment of the effect of high NA objectives to "see around" the fluorophore and therefore collect all three emission components F_x, F_y, F_z leads to a slightly more complex description than Eq. 14 [301, 306, 308], this empirical approach is attractive due to its simplicity and similarity with that of a collimated beam and has worked well in our laboratory and others [246]. The empirical constant z is a function of the NA of the microscope objective and is chosen such that (i) a time-resolved fluorescence anisotropy decay starts at the correct initial anisotropy r_0 (as determined by spectroscopic measurements using collimated excitation light) and (ii) the total fluorescence intensity decay $F_{||}(t) + zF\perp(t)$ is the same as a decay collected using collimated beams with magic angle detection such that polarization contributions are removed [246]. The denominator is proportional to the total fluorescence emission, and G accounts for differences in the transmission and detection efficiencies of the imaging system at parallel and perpendicular polarization. If necessary, an appropriate background has to be subtracted [309]. Due to the nature of the photoselection for absorption and emission transition dipoles, multiphoton excitation provides a greater dynamic range for anisotropy measurements than single-photon excitation [310].

The depolarization of the fluorescence, i.e., the decay of the anisotropy r as a function of time, can either be due to the rotational diffusion of the fluorophore in its excited state before emission of a fluorescence photon or due to energy migration or homo-FRET:

(i) Rotational Diffusion

The rotational diffusion of the fluorophore in its excited state before emission of a fluorescence photon depends on its volume and the viscosity and temperature of its environment. For a spherical molecule, $r(t)$ decays as a single exponential and is related to the rotational correlation time θ according to

$$r(t) = (r_0 - r_\infty)e^{-t/\theta} + r_\infty \tag{15}$$

where r_0 is the initial anisotropy (maximum value is 0.4 for single-photon excitation) and r_∞ accounts for a restricted rotational mobility. $r_\infty = 0$ for freely rotating fluorophores, e.g., in isotropic, homogeneous solution. For a spherical molecule in an isotropic medium, θ is directly proportional to the viscosity η of the solvent and the hydrodynamic volume V of the rotating molecule:

$$\theta = \frac{\eta V}{kT} \tag{16}$$

where k is the Boltzmann constant and T the absolute temperature. Therefore, if the volume of the fluorophore is known, the rotational correlation time can report on the viscosity of the fluorophore's immediate environment. Alternatively, as the rotational diffusion can be slowed down by binding or sped up by cleavage, θ can yield information about the size of the tumbling unit. In addition, evidence of a hindered rotation of the fluorophore due to geometrical restrictions, e.g., in the cell membrane, can be gleaned from r_∞.

If the anisotropy r in Eq. 14 is calculated from the fluorescence intensities, rather than the decays, then the steady-state fluorescence anisotropy is obtained. This is related to the molecular parameters r_0, r_∞, τ and θ via the Perrin equation [69, 70]

$$r = \frac{r_0 - r_\infty}{1 + \frac{\tau}{\theta}} + r_\infty \tag{17}$$

where τ is the fluorescence lifetime, defined in Eq. 3 [311]. While the steady-state anisotropy r is relatively easy to measure, and in particular to image [292], it may not be unambiguous to interpret in the absence of time-resolved measurements.

Steady-state fluorescence anisotropy imaging has, for example, been used to study viscosity, enzyme activity or binding in cells [312–319], and DNA digestion [320] or to identify FRET between fluorescent proteins [321–325]. However, it is difficult to obtain information about a hindered rotational mobility as indicated by a non-zero r_∞, and time-resolved measurements are needed to determine this parameter.

Time-resolved fluorescence anisotropy has been used on cells for single-point measurements [313, 326–328] and for mapping solvent interactions in microfluidic devices [19], as well as the viscosity in the cell cytoplasm [309, 311, 329] and membrane [330].

In the brain, the speed with which neurotransmitters diffuse in the interstitial space contributes critically to the shaping of elementary signals transferred by neural circuits. Indeed, experimental alterations of extracellular medium viscosity could reveal a clear impact of the interstitial diffusion rate on neural signal formation, both inside and outside the synaptic cleft [331–336]. Furthermore, it has been suggested that medium microviscosity could influence rapid movements of protein domains during ion channel opening: in the squid giant axon, a 30–40% increase in the local viscosity slows down the gating time of sodium channels by more than twofold [337].

Similarly, rapid intracellular diffusion of molecular messengers in the protein-crowded microenvironment of small cellular compartments sets the rates of diffusion-limited cellular signaling cascades throughout the central nervous system. Cytosolic mobility and protein crowding have been demonstrated to play an important role in controlling the intracellular spread of molecular signals generated by synaptic signal exchange [338–341]. In the context of neural coding mechanisms, it would seem reasonable to suggest that understanding the mobility of small signaling molecules in the microenvironment of functional connections in the brain bears as much importance as deciphering their rapid reaction kinetics per se.

Measurements of bulk extracellular diffusion in the brain have a long history. An important advance came with the point-source iontophoresis technique [342], which has been used extensively in various brain areas (reviewed in [343]). It was subsequently complemented by imaging methods which analyze profiles of fluorescence indicators ejected from a point source [336, 344–347] also employing quantum dots as a diffusing probe [348]. Recent developments in the spot imaging of extracellular fluorescent probes using microfiber optics have improved spatial resolution of such methods to just a few microns [349, 350]. However, these approaches deal with the apparent diffusion speed which incorporates steric hindrance, or tissue tortuosity, arising from geometric obstacles such as cell walls and membranes of cellular organelles. Molecular mobility on the scale of local biochemical reactions, i.e., within the range of several nanometers, remains poorly understood.

Perhaps the most well-established experimental approach to gauge intra-cytosolic diffusion has been fluorescence recovery after photobleaching or FRAP (reviewed in [351]). Combining FRAP and real-time imaging of photoactivated molecular probes has been highly instrumental in unveiling spatiotemporal aspects of molecular reactions in small dendritic compartments of neurons in situ [338–341, 352]. Assuming a sufficiently rapid image acquisition rate, the spatial resolution of this method could be as good as the diffraction-limited resolution in the optical acquisition system. Even at this resolution level, however, estimated diffusion will incorporate the effect of macromolecular obstacles, intracellular organelles, and membrane geometry features, potentially masking the speed at which small molecules shuttle within nanoscopic cellular compartments. Time-resolved fluorescence anisotropy imaging (TR-FAIM) [309, 329] is ideally suited to enable diffusion monitoring at the molecular scale or in other words to gauge quasi-instantaneous molecular mobility.

In the absence of rotational diffusion, polarization-resolved measurements can be used to elucidate the orientation of fluorophores, e.g., in the membrane [353, 354], muscle fibers [355], or DNA [356]. In these cases, neither the depolarization due to Brownian rotational motion nor homo-FRET is measured, but rather the angle between the electric vector of the light exciting the sample and the transition dipole moment of the static fluorophore, thus yielding its orientation.

(ii) Energy Migration or Homo-FRET

FRET can occur if the absorption spectrum of the acceptor overlaps with the emission spectrum of the donor, the fluorophores are in close proximity, and their

orientation is favorable (i.e., orientation factor $\kappa^2 \neq 0$ [104, 357, 358]), as extensively discussed in reference [7]. These conditions can apply to fluorophores with a small Stokes shift and hence lead to the donor and acceptor being the same type of fluorophore. Thus, resonance energy transfer between the same types of fluorophore can take place, known as energy migration or homo-FRET. This phenomenon depolarizes the fluorescence emission [98] and has been exploited in single-point measurements and imaging, e.g., to monitor the proximity of isoforms of the glycosylphosphatidylinositol (GPI)-anchored folate receptor bound to a fluorescent analogue of folic acid to study lipid rafts [359, 360], to monitor actin polymerization [361], or to image the aggregation of protein α-synuclein, relevant for Parkinson's disease [362].

Time-resolved fluorescence anisotropy measurements to identify homo-FRET have be carried out to study conformational changes in G-protein-coupled receptors [363], dimerization [364], and quantification of protein cluster sizes [365–368]. It has also been used to show that a neuronal isoform of Venus-tagged calcium–calmodulin-dependent protein kinase II alpha (CaMKIIa) holoenzyme forms catalytic domain pairs and that glutamate receptor activation in neurons triggered an increase in anisotropy consistent with a structural transition from a paired to unpaired conformation [51, 369]. Moreover, time-resolved fluorescence anisotropy measurements have been employed to study the homodimerization of amyloid precursor protein at the plasma membrane, relevant for Alzheimer's disease [57]. In these cases, it is advantageous to have negligible rotational diffusion (the ratio τ/θ is small), so that homo-FRET can be identified.

For homo-FRET involving two fluorophores, and in the absence of any rotational diffusion, $r(t)$ decays as a single exponential and is related to the FRET rate ω according to [364–366, 368]

$$r(t) = (r_0 - r_\infty)e^{-2\omega t} + r_\infty \tag{18}$$

where r_0 is the initial anisotropy in the absence of rotation or energy transfer, as defined above, and r_∞ is the anisotropy at a long time after the excitation. While hetero-FRET between different donors and acceptors to identify protein interaction can routinely be imaged with FLIM, mapping energy migration or homo-FRET to identify protein dimerization requires polarization-resolved FLIM, i.e., TR-FAIM. The only way to detect homo-FRET is by polarization measurements, because homo-FRET does not affect spectra or fluorescence lifetime – as long as the fluorescence lifetime of both fluorophores is the same – and thus cannot be identified by intensity or lifetime methods [296]. If the fluorescence lifetimes of the two fluorophores are different, however, then FRET can be identified by fluorescence lifetime measurements [370, 371]. This has, for example, been done in the case of tryptophan to tryptophan homo-FRET in barnase, where the tryptophans are located in different environments yielding different fluorescent lifetimes [372].

Homo-FRET between fluorescent proteins can be extremely fast (a 2 ps transfer time has been quoted for yellow fluorescent protein [373]) which is an indicator of protein dimerization or oligomerization, and TR-FAIM is the only technique which

can image it (Only in the specific case of the Cerulean fluorescent protein, the fluorescence lifetime has been reported to change due to homo-FRET [374]).

Anisotropy imaging can be performed as steady-state or time-resolved measurements in the time domain or frequency domain using scanning or wide-field methods [32, 118, 291] and has been combined with spectral imaging [254]. Photon counting approaches are particularly attractive because of their excellent signal-to-noise ratio and single-photon sensitivity [108, 248–250].

The combination of TIRF with time-resolved fluorescence anisotropy measurements allows excitation with *s*- and *p*-polarized evanescent waves and provides spatial information on the fluorescence depolarization processes near an interface. This has, for example, facilitated the observation of the rotation of membrane dyes in and out of plane [375, 376]. TIRF has indeed been combined with TR-FAIM [57, 58].

Phasor Analysis and Bayesian Analysis

Conventional FLIM data analysis in the time domain relies on Levenberg–Marquardt fitting algorithms to fit the experimental data to a mathematical model, i.e., compare data and theory [251]. This is a standard procedure that has been used in fluorescence spectroscopy for many decades.

The recent development of phasor analysis for FLIM [377] allows the visualization of the decay data without a specific mathematical model (but it does require a calibration measurement with a known reference sample). Although originally developed for data analysis in the frequency domain, it is equally well applicable in the time domain and in particular for FLIM. Essentially, the fluorescence decay is Fourier transformed, and the real part is plotted versus the imaginary part for each pixel. The resulting data cloud (or clouds) is on the universal semicircle for single-exponential decays, and various quenching processes result in trajectories within (or even outside) this universal semicircle.

The recent development for Bayesian analysis is particularly relevant for fluorescence decays with a low number of photons [378]. The Bayesian approach allows a decay time estimation with a much narrower confidence limit than Levenberg–Marquardt fitting if low photon numbers are involved – as is the case more often than not in many FLIM experiments. If the photon numbers are high enough, then Bayesian fitting does not offer any advantages over conventional Levenberg–Marquardt fitting.

Detector developments

Apart from the development and improvement of various microscopy techniques, for example, by super-resolution, selective plane illumination, or adaptive optics, and apart from fluorescent probe and protein development, detector development is also an important aspect to advance the field. While solid-state detector arrays have been

used for frequency-domain FLIM [27], the recent development of single-photon avalanche diode (SPAD) array detectors with picosecond timing capabilities holds great promise for the advancement of time-resolved fluorescence microscopy – especially in view of the limitations of the variety of current FLIM implementations.

Wide-Field TCSPC

Wide-field photon counting imaging is a well-established low light level optical imaging technique in astronomy, both on the ground and in space. The Hubble Space Telescope's Faint Object Camera [379] and the European Space Agency's X-ray Multi-Mirror satellite (the most powerful X-ray telescope ever placed in orbit, launched in 1999) were fitted with a photon counting imaging optical monitor [380]. The technique has also been used in autoradiography [381], bioluminescence [382], and fluorescence imaging [383–385]. Wide-field photon counting imaging has some distinct advantages over direct CCD-based imaging, in particular the ability to time the arrival of photons. However, while this technique has single-photon sensitivity, its drawback is that it has only a limited time resolution given by the frame rate of the camera (milliseconds for video rate cameras) [386]. Despite recent efforts to reduce the time resolution to microseconds [384], this method is still far too slow for application to nanosecond fluorescence decay measurements – and yet microchannel plate (MCP) detectors routinely achieve picosecond timing resolution when used for TCSPC [246]. The solution is to employ an electronic readout rather than a phosphor, thus preserving picosecond timing capabilities. Different readout architectures for photon counting imaging detectors exist, such as crossed-delay line anodes, wedge and strip anodes, or quadrant anodes [36, 255]. Quadrant anode detectors and crossed-delay line anode detectors for wide-field imaging with picosecond timing resolution have been developed, thus enabling wide-field TCSPC with picosecond time resolution [387]. Conventional photon pileup restrictions still apply – they can only time a single photon per excitation cycle in the entire field of view – but these devices combine single-photon sensitivity with wide-field detection and picosecond timing resolution. They provide the high level of sensitivity required for single-molecule analysis while also enabling TCSPC-based fluorescence lifetime measurements and single quantum dot tracking without beam scanning [255, 388].

SPAD Arrays

CCD or CMOS cameras for the optical pulse round-trip delays for time-of-flight ranging or three-dimensional imaging have been under development since the mid-1990s. The strong similarities between these signals and the capture of fluorescence lifetime decays were identified by Esposito et al. in a proof-of-concept demonstration [389].

The first commercial solid-state camera development for scientific FLIM was reported recently, comprising 212 × 212 pixels at 17 μm pitch and 44% fill factor [390].

The pixel integrates both phases of the modulated fluorescence simultaneously by directing accumulated photocharge via dual transfer gates from the photogate to storage gates. The operating principle of this imager is very similar to that of various time-of-flight image sensors which have been demonstrated in CMOS implementations [391–393] and demonstrated to be suitable for FLIM [27].

These modulated detectors cannot rival the low-light performance and image resolution of electron-multiplied or intensified CCD systems or the single-photon sensitivity and timing resolution provided by photomultiplier tubes. The single-photon avalanche diode (SPAD), which was first realized in CMOS technology around 2003 [394], provides a solid-state detector combining high sensitivity and high timing resolution with array formats and multichannel timing. A number of gated SPAD pixel realizations for fluorescence lifetime have been reported [395, 396]. Line sensors allow a high fill factor by allowing pulse processing electronics to be placed below the detectors. Advanced realizations of these line sensors are beginning to emerge for time-resolved Raman spectroscopy [397].

The first time-resolved CMOS SPAD imagers placed the timing circuitry off-chip or off-focal plane requiring different degrees of time multiplexing [398, 399]. This is beneficial for fill factor but inefficient for low-light imaging due to the loss of photons at unaddressed pixel sites. Pixels with on-focal plane time-to-digital converter (TDC) were proposed in the MegaFrame EU project [400–402]. The pixels provide fully parallel TCSPC at the expense of a large pitch of 50 μm and low fill factor of 2%. The largest fully parallel SPAD array with 160 × 120 TCSPC channels was developed recently and has shown good TDC uniformity [403]. Recent work has moved the parallel TDC array off the focal plane providing 64 × 64 TCSPC channels operating at 100 frames per second [404]. Another sensor used 16 off-focal plane TDC channels to achieve 10% fill factor extending the conventional pileup limit to a photon rate of 10× the laser pulse rate [405]. This chip was the first to embed fluorescence lifetime calculation on-chip offering prospects for high dynamic range confocal scanning or fluorescence lifetime-activated cell sorting.

Two sensors composed of n-type metal oxide semiconductor logic-only, time-gated SPAD pixels of 25 μm pitch with fill factors of 4.5% and 20.8%, respectively, were reported recently in 0.35 μm high-voltage CMOS technology [401, 406]. More recently, Dutton et al. reported the first sub-10 μm pitch time-resolved SPAD pixels [407]. Analogue pixel electronics can provide simultaneously low pixel pitch and high fill factor and shows enormous promise for future time-resolved image sensors with the required levels of sensitivity and image resolution for microscopy.

The design of detectors and timing electronics on a single substrate inevitably provides compactness and large numbers of channels but compromises fill factor and SPAD performance (jitter, photon detection efficiency, afterpulsing, and dark count). Recent work by Antonioli et al. [408] has resulted in a 32-channel TCSPC system employing the hybrid integration of a custom 32 SPAD array with 32-channel active quench and time-to-analogue converter array. The timing resolution and detector characteristics are separately optimized providing the ultimate performance for physics and biomedical research.

The big advantage of these latest developments in SPAD array detector technology is that it allows independent photon arrival timing in each pixel of a 32 × 32 pixel array simultaneously. This is due to a time-to-digital converter in each pixel, with a 55 ps resolution. The new SPAD array technology thus combines the advantages of TCSPC detection with parallel pixel acquisition as in wide-field FLIM. This development can massively parallelize TCSPC detection and can overcome the conventional implementation of scanning a single beam with a single TCSPC detector. This new SPAD array technology offers a huge advantage over existing fluorescence lifetime and anisotropy measurement tools and could present a paradigm shift in our approach to dynamically monitoring protein interactions and sensing the biophysical environment in cells in real time.

SPAD array detectors have a small fill factor (<10%), because the majority of the area of each pixel is occupied by electronic circuits to perform the timing, with only a small light-sensitive area dedicated to the detection of photons. To fully exploit the parallel single-photon detection and timing capabilities of these detector arrays, the entire fluorescence signal is therefore best focused onto the light-sensitive area. The use of microlens arrays is a possible solution but may be impractical for this task. However, preliminary multifocal multibeam approaches have been successfully demonstrated to achieve this aim [409, 410].

Superconducting Detectors

In addition, detector technology based on devices exploiting superconductivity has the ability to detect single photons. Superconducting tunnel junction (STJ) detectors, transition edge sensors, and superconducting nanowire detectors go beyond the principles employed in semiconductor and photoelectronic vacuum devices, i.e., electron–hole pair generation and the photoelectric effect. While transition edge sensors are calorimeters that detect the energy of a photon deposited in the detector, superconducting tunnel junction detectors have superconducting photocathodes and rely on the photons separating the individual electrons in Cooper pairs which only have a milli-electronvolt binding energy. The resulting electrons tunnel through a thin layer beyond which they are picked up and amplified. The interesting feature of such detectors is that they have an intrinsic wavelength resolution – the detector can determine the wavelength of the detected photon without employing any filters, gratings, or prisms to disperse the light. In the case of STJs, this is given by the pulse height of the signal, i.e., the number of electrons generated. Moreover, they have a high quantum efficiency over a very large wavelength range from X-rays to infrared and low noise, but they need to be operated at liquid helium temperatures, i.e., below −270 °C. These devices have already been demonstrated to be able to measure the spectra of fluorescent dyes in solution [411] and as labels for DNA [412], but they have not been used for microscopy. The disadvantage is that they have a very long pulse rise time of micro- or milliseconds, so count rates in a single pixel are limited, but pixelated devices have been manufactured and used on telescopes for optical astronomy [413].

Superconducting nanowires, on the other hand, have a very fast pulse rise time and can count single photons at MHz count rates [414]. They also have very low noise but limited quantum efficiencies (which can be overcome by cavity resonators [415]) and no intrinsic wavelength resolution. They are based on meandering superconducting wires just below the transition temperature, as reviewed recently [416]. A photon deposits energy and heats up the wire so that the transition temperature is exceeded, and a pulse results. They have an excellent signal-to-noise ratio in the infrared and have recently been employed to detect singlet oxygen luminescence at 1270 nm, generated by photosensitizer Rose Bengal, with unprecedented sensitivity [417]. Although these devices have not yet been demonstrated for microscopy, they would be ideally suited as a single-point detector in confocal or multiphoton excitation microscopy with picosecond time resolution and high detection efficiency in the infrared.

Summary and Outlook

The power of fluorescence-based optical imaging to drive major discoveries in cell biology is universally recognized. It offers two principal advantages: light microscopy allows the observation of structures inside a living sample in real time, and cellular components or compartments may be observed through specific fluorescence labeling. The key point of FLIM lies in the ability to monitor the environment of a fluorophore largely independent of its concentration – so in addition to the position of the fluorophore, its biophysical environment can be sensed via the lifetime.

There are various implementations of FLIM, and, depending on the application, each has its advantages and drawbacks. The ideal fluorescence microscope would acquire the entire multidimensional fluorescence emission contour of intensity, position, lifetime, wavelength, and polarization in a single measurement, with single-photon sensitivity, maximum spatial resolution, and minimum acquisition time (Fig. 1). Needless to say, there is presently no technology with this unique combination of features, and to build one remains a challenge for instrumentation developers. The recent development of SPAD array detectors with picosecond timing capabilities holds great promise for the advancement of time-resolved fluorescence microscopy – especially in view of the limitations of the variety of current FLIM and TR-FAIM implementations. In the last few years, the potential power of fluorescence lifetime-based optical imaging has increased dramatically, and the development of 100% fill factor SPAD arrays should continue this trend.

Acknowledgments We would like to thank the UK's MRC, BBSRC, and EPSRC for funding.

References

1. Borst JW, Visser AJWG (2010) Fluorescence lifetime imaging microscopy in life sciences. Meas Sci Technol 21(10):102002
2. Berezin MY, Achilefu S (2010) Fluorescence lifetime measurements and biological imaging. Chem Rev 110(5):2641–2684

3. Becker W (2012) Fluorescence lifetime imaging – techniques and applications. J Microsc 247 (2):119–136
4. Wallrabe H, Periasamy A (2005) Imaging protein molecules using FRET and FLIM microscopy. Curr Opin Biotechnol 16(1):19–27
5. Chen Y, Mills JD, Periasamy A (2003) Protein localization in living cells and tissues using FRET and FLIM. Differentiation 71(9–10):528–541
6. Peter M, Ameer-Beg SM (2004) Imaging molecular interactions by multiphoton FLIM. Biol Cell 96(3):231–236
7. Jares-Erijman EA, Jovin TM (2003) FRET imaging. Nat Biotechnol 21(11):1387–1396
8. Duncan RR (2006) Fluorescence lifetime imaging microscopy (FLIM) to quantify protein-protein interactions inside cells. Biochem Soc Trans 34(5):679–682
9. Festy F, Ameer-Beg SM, Ng T, Suhling K (2007) Imaging proteins in vivo using fluorescence lifetime microscopy. Mol Biosyst 3(6):381–391
10. Pietraszewska-Bogiel A, Gadella TWJ (2011) FRET microscopy: from principle to routine technology in cell biology. J Microsc 241(2):111–118
11. Bird DK, Agg KM, Barnett NW, Smith TA (2007) Time-resolved fluorescence microscopy of gunshot residue: an application to forensic science. J Microsc Oxf 226(1):18–25
12. Ni T, Melton LA (1996) Two-dimensional gas-phase temperature measurements using fluorescence lifetime imaging. Appl Spectrosc 50(9):1112–1116
13. Ehn A, Johansson O, Bood J, Arvidsson A, Li B, Alden M (2011) Fluorescence lifetime imaging in a flame. Proc Combust Inst 33:807–813
14. Liaugaudas G, Collins AT, Suhling K, Davies G, Heintzmann R (2009) Luminescence-lifetime mapping in diamond. J Phys Condens Matter 21:364210, (7 pp)
15. Liaugaudas G, Davies G, Suhling K, Khan RUA, Evans DJF (2012) Luminescence lifetimes of neutral nitrogen-vacancy centres in synthetic diamond containing nitrogen. J Phys Condens Matter 24:435503 (5pp)
16. Magennis SW, Graham EM, Jones AC (2005) Quantitative spatial mapping of mixing in microfluidic systems. Angew Chem Int Ed 44(40):6512–6516
17. Benninger RKP, Koc Y, Hofmann O, Requejo-Isidro J, Neil MAA, French PMW, deMello AJ (2006) Quantitative 3D Mapping of Fluidic Temperatures within Microchannel Networks Using Fluorescence Lifetime Imaging. Anal Chem 78:2272–2278
18. Robinson T, Valluri P, Manning HB, Owen DM, Munro I, Talbot CB, Dunsby C, Eccleston JF, Baldwin GS, Neil MAA, de Mello AJ, French PMW (2008) Three-dimensional molecular mapping in a microfluidic mixing device using fluorescence lifetime imaging. Opt Lett 33(16):1887–1889
19. Benninger RKP, Hofmann O, McGinty J, Requejo-Isidro J, Munro I, Neil MAA, deMello AJ, French PMW (2005) Time-resolved fluorescence imaging of solvent interactions in microfluidic devices. Opt Express 13(16):6275–6285
20. Elder AD, Matthews SM, Swartling J, Yunus K, Frank JH, Brennan CM, Fisher AC, Kaminski CF (2006) The application of frequency-domain Fluorescence Lifetime Imaging Microscopy as a quantitative analytical tool for microfluidic devices. Opt Express 14(12):5456–5467
21. Graham EM, Iwai K, Uchiyama S, de Silva AP, Magennis SW, Jones AC (2010) Quantitative mapping of aqueous microfluidic temperature with sub-degree resolution using fluorescence lifetime imaging microscopy. Lab Chip 10(10):1267–1273
22. Redford GI, Majumdar ZK, Sutin JDB, Clegg RM (2005) Properties of microfluidic turbulent mixing revealed by fluorescence lifetime imaging. J Chem Phys 123(22):224504
23. Comelli D, D'Andrea C, Valentini G, Cubeddu R, Colombo C, Toniolo L (2004) Fluorescence lifetime imaging and spectroscopy as tools for nondestructive analysis of works of art. Appl Optics 43(10):2175–2183
24. Comelli D, Valentini G, Cubeddu R, Toniolo L (2005) Fluorescence lifetime imaging and Fourier transform infrared spectroscopy of Michelangelo's David. Appl Spectrosc 59 (9):1174–1181
25. Ge JH, Kuang CF, Lee SS, Kao FJ (2012) Fluorescence lifetime imaging with pulsed diode laser enabled stimulated emission. Opt Express 20(27):28216–28221

26. Lin PY, Lee SS, Chang CS, Kao FJ (2012) Long working distance fluorescence lifetime imaging with stimulated emission and electronic time delay. Opt Express 20(10):11445–11450
27. Esposito A (2012) Beyond range: innovating fluorescence microscopy. Remote Sens 4 (1):111–119
28. Togashi DM, Romao RIS, da Silva AMG, Sobral AJFN, Costa SMB (2005) Self-organization of a sulfonamido-porphyrin in Langmuir monolayers and Langmuir-Blodgett films. Phys Chem Chem Phys 7:3875–3884
29. Okabe K, Inada N, Gota C, Harada Y, Funatsu T, Uchiyama S (2012) Intracellular temperature mapping with a fluorescent polymeric thermometer and fluorescence lifetime imaging microscopy. Nat Commun 3:705
30. Bennet MA, Richardson PR, Arlt J, McCarthy A, Buller GS, Jones AC (2011) Optically trapped microsensors for microfluidic temperature measurement by fluorescence lifetime imaging microscopy. Lab Chip 11(22):3821–3828
31. Li Q, Ruckstuhl T, Seeger S (2004) Deep-UV laser-based fluorescence lifetime imaging microscopy of single molecules. J Phys Chem B 108(24):8324–8329
32. Suhling K (2006) Fluorescence Lifetime Imaging. In: Stephens D (ed) Cell Imaging. Scion, Bloxham, pp 219–245
33. Harris H (1999) The Birth of the Cell. Yale University Press, New Haven, p 212pp
34. Wouters FS (2006) The physics and biology of fluorescence microscopy in the life sciences. Contemp Phys 47(5):239–255
35. Amos WB, White JG (2003) How the confocal laser scanning microscope entered biological research. Biol Cell 95(6):335–342
36. Michalet X, Siegmund OHW, Vallerga J, Jelinsky P, Millaud JE, Weiss S (2007) Detectors for single-molecule fluorescence imaging and spectroscopy. J Mod Opt 54(2–3):239–281
37. Hadfield RH (2009) Single-photon detectors for optical quantum information applications. Nat Photonics 3(12):696–705
38. Buller GS, Collins RJ (2010) Single-photon generation and detection. Meas Sci Technol 21 (1):012002
39. Hungerford G, Birch DJS (1996) Single-photon timing detectors for fluorescence lifetime spectroscopy. Meas Sci Technol 7(2):121–135
40. Eisaman MD, Fan J, Migdall A, Polyakov SV (2011) Invited review article: single-photon sources and detectors. Rev Sci Instrum 82(7):071101
41. Shaner NC, Patterson GH, Davidson MW (2007) Advances in fluorescent protein technology. J Cell Sci 120(24):4247–4260
42. Smith GE (2009) The invention and early history of the CCD. Nucl Instrum Methods Phys Res A 607(1):1–6
43. Hirvonen LM, Smith TA (2011) Imaging on the nanoscale: super-resolution fluorescence microscopy. Aust J Chem 64(1):41–45
44. Heintzmann R, Ficz G (2006) Breaking the resolution limit in light microscopy. Brief Funct Genomic Proteomic 5:289–301
45. Galbraith CG, Galbraith JA (2011) Super-resolution microscopy at a glance. J Cell Sci 124 (10):1607–1611
46. Venetta BD (1959) Microscope phase fluorometer for determining the fluorescence lifetimes of fluorochromes. Rev Sci Instrum 30(6):450–457
47. Bugiel I, König K, Wabnitz H (1989) Investigation of cells by fluorescence laser scanning microscopy with subnanosecond time resolution. Lasers Life Sci 3(1):47–53
48. Wang XF, Uchida T, Minami S (1989) A fluorescence lifetime distribution measurement system based on phase-resolved detection using an image dissector tube. Appl Spectrosc 43 (5):840–845
49. Breusegem SY, Levi M, Barry NP (2006) Fluorescence correlation spectroscopy and fluorescence lifetime imaging microscopy. Nephron J 103(2):e41–e49
50. Becker W, Bergmann A, Haustein E, Petrasek Z, Schwille P, Biskup C, Kelbauskas L, Benndorf K, Klöcker N, Anhut T, Riemann I, König K (2006) Fluorescence lifetime images

and correlation spectra obtained by multidimensional time-correlated single photon counting. Microsc Res Tech 69(3):186–195
51. Nguyen TA, Sarkar P, Veetil JV, Koushik SV, Vogel SS (2012) Fluorescence polarization and fluctuation analysis monitors subunit proximity, stoichiometry, and protein complex hydrodynamics. Plos One 7(5):e38209
52. Kwak ES, Kang TJ, Bout DAV (2001) Fluorescence lifetime imaging with near-field scanning optical microscopy. Anal Chem 73(14):3257–3262
53. Micic M, Hu DH, Suh YD, Newton G, Romine M, Lu HP (2004) Correlated atomic force microscopy and fluorescence lifetime imaging of live bacterial cells. Colloids Surf B Biointerfaces 34(4):205–212
54. Levitt JA, Chung PH, Alibhai DR, Suhling K (2011) Simultaneous measurements of fluorescence lifetimes, anisotropy and FRAP recovery curves. In: SPIE Proc 7902:79020Y.
55. Roberti MJ, Jovin TM, Jares-Erijman E (2011) Confocal Fluorescence anisotropy and FRAP imaging of alpha-synuclein amyloid aggregates in living cells. Plos One 6(8):e23338
56. Vitali M, Reis M, Friedrich T, Eckert H-J (2010) A wide-field multi-parameter FLIM and FRAP setup to investigate the fluorescence emission of individual living cyanobacteria. SPIE Proc 7376:737610
57. Devauges V, Marquer C, Lecart S, Cossec JC, Potier MC, Fort E, Suhling K, Leveque-Fort S (2012) Homodimerization of amyloid precursor protein at the plasma membrane: a homo-FRET study by time-resolved fluorescence anisotropy imaging. Plos One 7(9):e44434
58. Bruns T, Strauss WSL, Schneckenburger H (2008) Total internal reflection fluorescence lifetime and anisotropy screening of cell membrane dynamics. J Biomed Opt 13(4):041317
59. Auksorius E, Boruah BR, Dunsby C, Lanigan PMP, Kennedy G, Neil MAA, French PMW (2008) Stimulated emission depletion microscopy with a supercontinuum source and fluorescence lifetime imaging. Opt Lett 33(2):113–115
60. Lin PY, Lin YC, Chang CS, Kao FJ (2013) Fluorescence lifetime imaging microscopy with subdiffraction-limited resolution. Jpn J Appl Phys 52(2):028004
61. Slepkov AD, Ridsdale A, Wan HN, Wang MH, Pegoraro AF, Moffatt DJ, Pezacki JP, Kao FJ, Stolow A (2011) Forward-collected simultaneous fluorescence lifetime imaging and coherent anti-Stokes Raman scattering microscopy. J Biomed Opt 16(2):021103
62. McGinty J, Stuckey DW, Soloviev VY, Laine R, Wylezinska-Arridge M, Wells DJ, Arridge SR, French PMW, Hajnal JV, Sardini A (2011) In vivo fluorescence lifetime tomography of a FRET probe expressed in mouse. Biomed Opt Express 2(7):1907–1917
63. Valeur B, Berberan-Santos M (2011) A brief history of fluorescence and phosphorescence before the emergence of quantum theory. J Chem Educ 88:731–738
64. Stokes GG (1852) On the change of refrangibility of light. Philos Trans R Soc Lond 142:463–562
65. Stokes GG (1853) On the change of refrangibility of light II. Phil Trans R Soc London 143:385–396
66. Malley M (1991) A heated controversy on cold light. Arch Hist Exact Sci 42(2):173–186
67. Stern O, Volmer M (1919) Über die Abklingungszeit der Fluoreszenz. Phys Z 20:183–188
68. Gaviola E (1926) Die Abklingungszeiten der Fluoreszenz von Farbstofflösungen. Ann Phys 386(23):681–710
69. Lakowicz JR (2006) Principles of fluorescence spectroscopy, 3rd edn. Springer, New York
70. Valeur B, Berberan-Santos MN (2012) Molecular fluorescence. Principles and applications, 2nd edn. Wiley, Weinheim
71. Sauer M, Hofkens J, Enderlein J (2011) Handbook of fluorescence spectroscopy and imaging. Wiley-VCH, Weinheim
72. Goldys EM (2009) Fluorescence applications in biotechnology and life sciences. Wiley-Blackwell, Hoboken
73. Jablonski A (1935) Über den Mechanismus der Photolumineszenz von Farbstoffphosphoren. Z Phys 94:38–46

74. Kasha M (1950) Characterization of electronic transitions in complex molecules. Discuss Faraday Soc 9:14–19
75. Strickler SJ, Berg RA (1962) Relationship between absorption intensity and fluorescence lifetime of molecules. J Chem Phys 37(4):814–820
76. Einstein A (1917) Zur Quantentheorie der Strahlung. Phys Z 18:121–128
77. Einstein A (1916) Strahlungsemission und -absorption nach der Quantentheorie. Ber Deutsch Phys Ges 13–14:3128–3323
78. Toptygin D, Savtchenko RS, Meadow ND, Roseman S, Brand L (2002) Effect of the solvent refractive index on the excited-state lifetime of a single tryptophan residue in a protein. J Phys Chem B 106(14):3724–3734
79. Toptygin D (2003) Effects of the solvent refractive index and its dispersion on the radiative decay rate and extinction coefficient of a fluorescent solute. J Fluoresc 13(3):201–219
80. Istratov AA, Vyvenko OF (1999) Exponential analysis in physical phenomena. Rev Sci Instrum 70(2):1233–1257
81. Zollinger H (2003) Color chemistry: syntheses, properties, and applications of organic dyes and pigments. Helvetica Chimica Acta, Zurich
82. Resch-Genger U, Grabolle M, Cavaliere-Jaricot S, Nitschke R, Nann T (2008) Quantum dots versus organic dyes as fluorescent labels. Nat Methods 5(9):763–775
83. Howes P, Green M, Levitt J, Suhling K, Hughes M (2010) Phospholipid encapsulated semiconducting polymer nanoparticles: their use in cell imaging and protein attachment. J Am Chem Soc 132(11):3989–3996
84. Green M, Howes P, Berry C, Argyros O, Thanou M (2009) Simple conjugated polymer nanoparticles as biological labels. Proc R Soc Math Phys Eng Sci 465 (2109):2751–2759
85. Faklaris O, Joshi V, Irinopoulou T, Tauc P, Sennour M, Girard H, Gesset C, Arnault JC, Thorel A, Boudou JP, Curmi PA, Treussart F (2009) Photoluminescent diamond nanoparticles for cell labeling: study of the uptake mechanism in mammalian cells. ACS Nano 3 (12):3955–3962
86. Neugart F, Zappe A, Jelezko F, Tietz C, Boudou JP, Krueger A, Wrachtrup J (2007) Dynamics of diamond nanoparticles in solution and cells. Nano Lett 7(12):3588–3591
87. Mohan N, Chen CS, Hsieh HH, Wu YC, Chang HC (2010) In vivo imaging and toxicity assessments of fluorescent nanodiamonds in *Caenorhabditis elegans*. Nano Lett 10 (9):3692–3699
88. Kuo Y, Hsu T-Y, Wu Y-C, Hsu J-H, Chang H-C (2013) Fluorescence lifetime imaging microscopy of nanodiamonds in vivo. In: SPIE Proc 8635:863503
89. Edmonds AM, Sobhan MA, Sreenivasan VKA, Grebenik EA, Rabeau JR, Goldys EM, Zvyagin AV (2013) Nano-ruby: a promising fluorescent probe for background-free cellular imaging. Part Part Syst Charact 30(6):506–513
90. Sreenivasan VKA, Zvyagin AV, Goldys EM (2013) Luminescent nanoparticles and their applications in the life sciences. J Phys Condens Matter 25(19)
91. Green M (2004) Semiconductor quantum dots as biological imaging agents. Angew Chem 43 (32):4129–4131
92. Grecco HE, Lidke KA, Heintzmann R, Lidke DS, Spagnuolo C, Martinez OE, Jares-Erijman EA, Jovin TM (2004) Ensemble and single particle photophysical proper-ties (Two-photon excitation, anisotropy, FRET, lifetime, spectral conversion) of commercial quantum dots in solution and in live cells. Microsc Res Tech 65(4–5):169–179
93. Michalet X, Pinaud FF, Bentolila LA, Tsay JM, Doose S, Li JJ, Sundaresan G, Wu AM, Gambhir SS, Weiss S (2005) Quantum dots for live cells, in vivo imaging, and diagnostics. Science 307(5709):538–544
94. Chudakov DM, Matz MV, Lukyanov S, Lukyanov KA (2010) Fluorescent proteins and their applications in imaging living cells and tissues. Physiol Rev 90(3):1103–1163
95. Elson D et al (2004) Time-domain fluorescence lifetime imaging applied to biological tissue. Photochem Photobiol Sci 3(8):795–801

96. Urayama P, Mycek M-A (2003) Fluorescence lifetime imaging microscopy of endogenous biological fluorescence. In: Mycek M-A, Pogue BW (eds) Handbook of biomedical fluorescence. Marcel Dekker, New York
97. Ahmed Z, Lin CC, Suen KM, Melo FA, Levitt JA, Suhling K, Ladbury JE (2013) Grb2 controls phosphorylation of FGFR2 by inhibiting receptor kinase and Shp2 phosphatase activity. J Cell Biol 200(4):493–504
98. Förster T (1946) Energiewanderung und Fluoreszenz. Naturwissenschaften 33(6):167–175, translated into English by Suhling K (2012) J Biomed Opt 17(1):011002
99. Ogilby PR (2010) Singlet oxygen: there is indeed something new under the sun. Chem Soc Rev 39(8):3181–3209
100. Dixon JM, Taniguchi M, Lindsey JS (2005) PhotochemCAD 2: a refined program with accompanying spectral databases for photochemical calculations. Photochem Photobiol 81 (1):212–213
101. Du H, Fuh RCA, Li J, Corkan LA, Lindsey JS (1998) PhotochemCAD: a computer-aided design and research tool in photochemistry. Photochem Photobiol 68(2):141–142
102. Stryer L (1978) Fluorescence energy transfer as a spectroscopic ruler. Annu Rev Biochem 47:819–846
103. Stryer L, Haugland RP (1967) Energy transfer: a spectroscopic ruler. Proc Natl Acad Sci U S A 58:719–726
104. Dos Remedios CG, Moens PDJ (1995) Fluorescence resonance energy transfer spectroscopy is a reliable "Ruler" for measuring structural changes in proteins. Dispelling the problem of the unknown orientation factor. J Struct Biol 115(2):175–185
105. Hunt J, Keeble AH, Dale RE, Corbett MK, Beavil RL, Levitt J, Swann MJ, Suhling K, Ameer-Beg S, Sutton BJ, Beavil AJ (2012) A fluorescent biosensor reveals conformational changes in human immunoglobulin E Fc. Implications for mechanisms of receptor binding, inhibition and allergen recognition. J Biol Chem 287(21):17459–17470
106. Hötzer B, Ivanov R, Altmeier S, Kappl R, Jung G (2011) Determination of copper(II) ion concentration by lifetime measurements of green fluorescent protein. J Fluoresc 21 (6):2143–2153
107. Miyawaki A, Llopis J, Helm R, McCaffery JM, Adams JA, Ikura M, Tsien RY (1997) Fluorescent indicators for Ca^{2+} based on green fluorescent proteins and calmodulin. Nature 388(6645):882–887
108. Pelet S, Previte MJR, So PTC (2006) Comparing the quantification of Förster resonance energy transfer measurement accuracies based on intensity, spectral, and lifetime imaging. J Biomed Opt 11(3):034017
109. Thaler C, Koushik SV, Blank PS, Vogel SS (2005) Quantitative multiphoton spectral imaging and its use for measuring resonance energy transfer. Biophys J 89:2736–2749
110. Fiserova E, Kubala M (2012) Mean fluorescence lifetime and its error. J Luminescence 132 (8):2059–2064
111. Sillen A, Engelborghs Y (1998) The correct use of "average" fluorescence parameters. Photochem Photobiol 67(5):475–486
112. Suhling K, Siegel J, Phillips D, French PMW, Lévêque-Fort S, Webb SED, Davis DM (2002) Imaging the environment of green fluorescent protein. Biophys J 83(6):3589–3595
113. Uskova MA, Borst J, Hink MA, van Hoek A, Schots A, Klyachko AL, Visser AJWG (2000) Fluorescence dynamics of green fluorescent protein in AOT reversed micelles. Biophys Chem 87:73–84
114. Heikal AA, Hess ST, Webb WW (2001) Multiphoton molecular spectroscopy and excited-state dynamics of enhanced green fluorescent protein (EGFP): acid–base specificity. Chem Phys 274(1):37–55
115. Cotlet M, Hofkens J, Maus M, Gensch T, van der Auweraer M, Michiels J, Dirix G, van Guyse M, Vanderleyden J, Visser AJWG, de Schryver FC (2001) Excited state dynamics in the enhanced green fluorescent protein mutant probed by picosecond time-resolved single photon counting spectroscopy. J Phys Chem B 105(21):4999–5006

116. Jovin TM, Arndt-Jovin DJ (1989) FRET microscopy: digital imaging of fluorescence resonance energy transfer. In: Kohen E, Hirschberg JG, Ploem JS (eds) Cell structure and function by microspectrofluorometry. Academic, London, pp 99–117
117. Fernandez SM, Berlin RD (1976) Cell-surface distribution of lectin receptors determined by resonance energy-transfer. Nature 264(5585):411–415
118. Suhling K, French PMW, Phillips D (2005) Time-resolved fluorescence microscopy. Photochem Photobiol Sci 4:13–22
119. Shaner NC, Steinbach PA, Tsien RY (2005) A guide to choosing fluorescent proteins. Nat Methods 2(12):905–909
120. Zimmer M (2002) Green fluorescent protein (GFP): applications, structure, and related photophysical behavior. Chem Rev 102(3):759–781
121. Haidekker MA, Nipper M, Mustafic A, Lichlyter D, Dakanali M, Theodorakis EA (2010) Dyes with segmental mobility: molecular rotors. In: Demchenko AP (ed) Advanced fluorescence reporters in chemistry and biology I. Fundamentals and molecular design. Springer, Berlin/Heidelberg, pp 267–308
122. Haidekker MA, Theodorakis EA (2007) Molecular rotors-fluorescent biosensors for viscosity and flow. Org Biomol Chem 5(11):1669–1678
123. Kuimova MK (2012) Molecular rotors image intracellular viscosity. Chimia 66(4):159–165
124. Kuimova MK (2012) Mapping viscosity in cells using molecular rotors. Phys Chem Chem Phys 14(37):12671–12686
125. Uzhinov BM, Ivanov VL, Melnikov MY (2011) Molecular rotors as luminescence sensors of local viscosity and viscous flow in solutions and organized systems. Russ Chem Rev 80 (12):1179–1190
126. Förster T, Hoffmann G (1971) Die Viskositätsabhängigkeit der Fluoreszenzquantenausbeuten einiger Farbstoffsysteme. Z Phys Chem Neue Folge 75:63–76
127. Loutfy RO (1986) Fluorescence probes for polymer free-volume. Pure Appl Chem 58 (9):1239–1248
128. Rei A, Hungerford G, Ferreira MIC (2008) Probing local effects in silica sol–gel media by fluorescence spectroscopy of p-DASPMI. J Phys Chem B 112(29):8832–8839
129. Hungerford G, Allison A, McLoskey D, Kuimova MK, Yahioglu G, Suhling K (2009) Monitoring sol-to-gel transitions via fluorescence lifetime determination using viscosity sensitive fluorescent probes. J Phys Chem B 113(35):12067–12074
130. Law KY (1981) Fluorescence probe for micro-environments – a new probe for micelle solvent parameters and premicellar aggregates. Photochem Photobiol 33(6):799–806
131. Lu J, Liotta CL, Eckert CA (2003) Spectroscopically probing microscopic solvent properties of room-temperature ionic liquids with the addition of carbon dioxide. J Phys Chem A 107 (19):3995–4000
132. Gutkowski KI, Japas ML, Aramendia PF (2006) Fluorescence of dicyanovinyl julolidine in a room-temperature ionic liquid. Chem Phys Lett 426(4–6):329–333
133. Paul A, Samanta A (2008) Free volume dependence of the internal rotation of a molecular rotor probe in room temperature ionic liquids. J Phys Chem B 112(51):16626–16632
134. Haidekker MA, Tsai AG, Brady T, Stevens HY, Frangos JA, Theodorakis E, Intaglietta M (2002) A novel approach to blood plasma viscosity measurement using fluorescent molecular rotors. Am J Phys Heart Circ Physiol 282(5):H1609–H1614
135. Kung CE, Reed JK (1986) Microviscosity measurements of phospholipid bilayers using fluorescent dyes that undergo torsional relaxation. Biochemistry 25:6114–6121
136. Nipper ME, Dakanali M, Theodorakis EA, Haidekker MA (2010) Detection of liposome membrane viscosity perturbations with ratiometric molecular rotors. Biochimie 93:988–994
137. Kung CE, Reed JK (1989) Fluorescent molecular rotors – a new class of probes for tubulin structure and assembly. Biochemistry 28(16):6678–6686
138. Kuimova MK, Yahioglu G, Levitt JA, Suhling K (2008) Molecular rotor measures viscosity of live cells via fluorescence lifetime imaging. J Am Chem Soc 130(21):6672–6673

139. Levitt JA, Kuimova MK, Yahioglu G, Chung PH, Suhling K, Phillips D (2009) Membrane-bound molecular rotors measure viscosity in live cells via fluorescence lifetime imaging. J Phys Chem C 113(27):11634–11642
140. Peng X, Yang Z, Wang J, Fan J, He Y, Song F, Wang B, Sun S, Qu J, Qi J, Yan M (2011) Fluorescence ratiometry and fluorescence lifetime imaging: using a single molecular sensor for dual mode imaging of cellular viscosity. J Am Chem Soc 133:6626–6635
141. Wandelt B, Cywinski P, Darling GD, Stranix BR (2005) Single cell measurement of micro-viscosity by ratio imaging of fluorescence of styrylpyridinium probe. Biosens Bioelectron 20 (9):1728–1736
142. Haidekker MA, Ling T, Anglo M, Stevens HY, Frangos JA, Theodorakis EA (2001) New fluorescent probes for the measurement of cell membrane viscosity. Chem Biol 8(2): 123–131
143. Luby-Phelps K, Mujumdar S, Mujumdar R, Ernst LA, Galbraith W, Waggoner AS (1993) A novel fluorescence ratiometric method confirms the low solvent viscosity of the cytoplasm. Biophys J 65(1):236–242
144. Battisti A, Panettieri S, Abbandonato G, Jacchetti E, Cardarelli F, Signore G, Beltram F, Bizzarri R (2013) Imaging intracellular viscosity by a new molecular rotor suitable for phasor analysis of fluorescence lifetime. Anal Bioanal Chem 405(19):6223–6233
145. Kuimova MK, Botchway SW, Parker AW, Balaz M, Collins HA, Anderson HL, Suhling K, Ogilby PR (2009) Imaging intracellular viscosity of a single cell during photoinduced cell death. Nat Chem 1:69–73
146. Haidekker M, Brady TP, Lichlyter D, Theodorakis EA (2006) A ratiometric fluorescent viscosity sensor. J Am Chem Soc 128:398–399
147. Wandelt B, Mielniczak A, Turkewitsch P, Darling GD, Stranix BR (2003) Substituted 4-[4-(dimethylamino)styryl] pyridinium salt as a fluorescent probe for cell microviscosity. Biosens Bioelectron 18(4):465–471
148. Ghiggino KP, Hutchison JA, Langford SJ, Latter MJ, Lee MAP, Lowenstern PR, Scholes C, Takezaki M, Wilman BE (2007) Porphyrin-based molecular rotors as fluorescent probes of nanoscale environments. Adv Funct Mater 17(5):805–813
149. Hosny NA, Mohamedi G, Rademeyer P, Owen J, Wu Y, Tang MX, Eckersley RJ, Stride E, Kuimova MK (2013) Mapping microbubble viscosity using fluorescence lifetime imaging of molecular rotors. Proc Natl Acad Sci U S A 110(23):9225–9230
150. Loison P, Hosny NA, Gervais P, Champion D, Kuimova MK, Perrier-Cornet JM (2013) Direct investigation of viscosity of an atypical inner membrane of *Bacillus* spores: a molecular rotor/FLIM study. Biochim Biophys Acta 1828(11):2436–2443
151. Mendels DA, Graham EM, Magennis SW, Jones AC, Mendels F (2008) Quantitative comparison of thermal and solutal transport in a T-mixer by FLIM and CFD. Microfluid Nanofluid 5(5):603–617
152. Treanor B, Lanigan PM, Suhling K, Schreiber T, Munro I, Neil MA, Phillips D, Davis DM, French PMW (2005) Imaging fluorescence lifetime heterogeneity applied to GFP-tagged MHC protein at an immunological synapse. J Microsc 217(1):36–43
153. Tregidgo C, Levitt JA, Suhling K (2008) Effect of refractive index on the fluorescence lifetime of green fluorescent protein. J Biomed Opt 13:031218
154. Ma YJ, Rajendran P, Blum C, Cesa Y, Gartmann N, Bruhwiler D, Subramaniam V (2011) Microspectroscopic analysis of green fluorescent proteins infiltrated into mesoporous silica nanochannels. J Colloid Interface Sci 356(1):123–130
155. van Manen HJ, Verkuijlen P, Wittendorp P, Subramaniam V, van den Berg TK, Roos D, Otto C (2008) Refractive index sensing of green fluorescent proteins in living cells using fluorescence lifetime imaging microscopy. Biophys J 94:L67–L69
156. Pliss A, Zhao LL, Ohulchanskyy TY, Qu JL, Prasad PN (2012) Fluorescence lifetime of fluorescent proteins as an intracellular environment probe sensing the cell cycle progression. ACS Chem Biol 7(8):1385–1392

157. Nakabayashi T, Nagao I, Kinjo M, Aoki Y, Tanaka M, Ohta N (2008) Stress-induced environmental changes in a single cell as revealed by fluorescence lifetime imaging. Photochem Photobiol Sci 7(6):671–674
158. Fort E, Gresillon S (2008) Surface enhanced fluorescence. J Phys D Appl Phys 41(1):013001
159. Lakowicz JR (2005) Radiative decay engineering 5: metal-enhanced fluorescence and plasmon emission. Anal Biochem 337(2):171–194
160. Barnes WL (1998) Fluorescence near interfaces: the role of photonic mode density. J Mod Opt 45(4):661–699
161. Teixeira R, Paulo PMR, Viana AS, Costa SMB (2011) Plasmon-enhanced emission of a phthalocyanine in polyelectrolyte films induced by gold nanoparticles. J Phys Chem C 115 (50):24674–24680
162. Cade NI, Fruhwirth G, Archibald SJ, Ng T, Richards D (2010) A cellular screening assay using analysis of metal-modified fluorescence lifetime. Biophys J 98(11):2752–2757
163. Kawata S, Inouye Y, Ichimura T (2004) Near-field optics and spectroscopy for molecular nano-imaging. Sci Prog 87(1):25–49
164. Cade NI, Fruhwirth GO, Ng T, Richards D (2013) Plasmon-assisted super-resolution axial distance sensitivity in fluorescence cell imaging. J Phys Chem Lett 4(20):3402–3406
165. Berndt M, Lorenz M, Enderlein J, Diez S (2010) Axial nanometer distances measured by fluorescence lifetime imaging microscopy. Nano Lett 10(4):1497–1500
166. Pickup JC, Zhi ZL, Khan F, Saxl T, Birch DJS (2008) Nanomedicine and its potential in diabetes research and practice. Diabetes Metab Res Rev 24(8):604–610
167. Saxl T, Khan F, Matthews DR, Zhi ZL, Rolinski O, Ameer-Beg S, Pickup J (2009) Fluorescence lifetime spectroscopy and imaging of nano-engineered glucose sensor microcapsules based on glucose/galactose-binding protein. Biosens Bioelectron 24(11):3229–3234
168. Saxl T, Khan F, Ferla M, Birch D, Pickup J (2011) A fluorescence lifetime-based fibre-optic glucose sensor using glucose/galactose-binding protein. Analyst 136(5):968–972
169. Biskup C, Gensch T (2014) Fluorescence lifetime imaging of ions in biological tissues. In: Elson D, French PWM, Marcu L (eds) Fluorescence lifetime spectroscopy and imaging. Principles and applications in biomedical diagnostics. Taylor & Francis, Boca Raton
170. Lakowicz JR, Szmacinski H, Nowaczyk K, Lederer WJ (1994) Fluorescence lifetime imaging of intracellular calcium in COS cells using Quin-2. Cell Calcium 15(1):7–27
171. Lakowicz JR, Szmacinski H, Nowaczyk K, Johnson ML (1992) Fluorescence lifetime imaging of calcium using Quin-2. Cell Calcium 13(3):131–147
172. Herman B, Wodnicki P, Kwon S, Periasamy A, Gordon GW, Mahajan N, Xue Feng W (1997) Recent developments in monitoring calcium and protein interactions in cells using fluorescence lifetime microscopy. J Fluoresc 7(1):85–92
173. Celli A, Sanchez S, Behne M, Hazlett T, Gratton E, Mauro T (2010) The epidermal Ca^{2+} gradient: measurement using the phasor representation of fluorescent lifetime imaging. Biophys J 98(5):911–921
174. Sanders R, Gerritsen HC, Draaijer A, Houpt PM, Levine YK (1994) Fluorescence lifetime imaging of free calcium in single cells. Bioimaging 2:131–138
175. Lahn M, Dosche C, Hille C (2011) Two-photon microscopy and fluorescence lifetime imaging reveal stimulus-induced intracellular Na^{+} and Cl^{-} changes in cockroach salivary acinar cells. Am J Physiol Cell Physiol 300(6):C1323–C1336
176. Kaneko H, Putzier I, Frings S, Kaupp UB, Gensch T (2004) Chloride accumulation in mammalian olfactory sensory neurons. J Neurosci 24(36):7931–7938
177. Gilbert D, Franjic-Wurtz C, Funk K, Gensch T, Frings S, Mohrlen F (2007) Differential maturation of chloride homeostasis in primary afferent neurons of the somatosensory system. Int J Dev Neurosci 25(7):479–489
178. Hötzer B, Ivanov R, Brumbarova T, Bauer P, Jung G (2012) Visualization of Cu^{2+}uptake and release in plant cells by fluorescence lifetime imaging microscopy. FEBS J 279(3): 410–419

179. Szmacinski H, Lakowicz JR (1999) Potassium and sodium measurements at clinical concentrations using phase-modulation fluorometry. Sensors Actuators B Chem 60(1):8–18
180. Szmacinski H, Lakowicz JR (1996) Fluorescence lifetime characterization of magnesium probes: improvement of Mg^{2+} dynamic range and sensitivity using phase-modulation fluorometry. J Fluoresc 6:83–85
181. Carlsson K, Liljeborg A, Andersson RM, Brismar H (2000) Confocal pH imaging of microscopic specimens using fluorescence lifetimes and phase fluorometry: influence of parameter choice on system performance. J Microsc 199(2):106–114
182. Sanders R, Draaijer A, Gerritsen HC, Houpt PM, Levine YK (1995) Quantitative pH imaging in cells using confocal fluorescence lifetime imaging microscopy. Anal Biochem 227:302–308
183. Lin HJ, Herman P, Lakowicz JR (2003) Fluorescence lifetime-resolved pH imaging of living cells. Cytometry 52A:77–89
184. Behne MJ, Meyer JW, Hanson KM, Barry NP, Murata S, Crumrine D, Clegg RW, Gratton E, Holleran WM, Elias PM (2002) NHE1 regulates the stratum corneum permeability barrier homeostasis. Microenvironment acidification assessed with fluorescence lifetime imaging. J Biol Chem 277(49):47399–47406
185. Hanson KM, Behne MJ, Barry NP, Mauro TM, Gratton E, Clegg RM (2002) Two-photon fluorescence lifetime imaging of the skin stratum corneum pH gradient. Biophys J 83 (3):1682–1690
186. Nakabayashi T, Wang HP, Kinjo M, Ohta N (2008) Application of fluorescence lifetime imaging of enhanced green fluorescent protein to intracellular pH measurements. Photochem Photobiol Sci 7(6):668–670
187. Ogikubo S, Nakabayashi T, Adachi T, Islam MS, Yoshizawa T, Kinjo M, Ohta N (2011) Intracellular pH sensing using autofluorescence lifetime microscopy. J Phys Chem B 115 (34):10385–10390
188. Estrada AD, Ponticorvo A, Ford TN, Dunn AK (2008) Microvascular oxygen quantification using two-photon microscopy. Opt Lett 33(10):1038–1040
189. Finikova OS, Lebedev AY, Aprelev A, Troxler T, Gao F, Garnacho C, Muro S, Hochstrasser RM, Vinogradov SA (2008) Oxygen microscopy by two-photon-excited phosphorescence. Chemphyschem 9(12):1673–1679
190. Hosny NA, Lee DA, Knight MM (2012) Single photon counting fluorescence lifetime detection of pericellular oxygen concentrations. J Biomed Opt 17:016007
191. Gerritsen HC, Sanders R, Draaijer A, Ince C, Levine YK (1997) Fluorescence lifetime imaging of oxygen in living cells. J Fluoresc 7(1):11–16
192. Choi H, Tzeranis DS, Cha JW, Clemenceau P, de Jong SJG, van Geest LK, Moon JH, Yannas IV, So PTC (2012) 3D-resolved fluorescence and phosphorescence lifetime imaging using temporal focusing wide-field two-photon excitation. Opt Express 20(24):26219–26235
193. Cicchi R, Pavone FS (2011) Non-linear fluorescence lifetime imaging of biological tissues. Anal Bioanal Chem 400(9):2687–2697
194. Ghukasyan VV, Kao FJ (2009) Monitoring cellular metabolism with fluorescence lifetime of reduced nicotinamide adenine dinucleotide. J Phys Chem C 113(27):11532–11540
195. Lakowicz JR, Szmacinski H, Nowaczyk K, Johnson ML (1992) Fluorescence lifetime imaging of free and protein-bound NADH. Proc Natl Acad Sci U S A 89(4):1271–1275
196. Mayevsky A, Chance B (2007) Oxidation-reduction states of NADH in vivo: From animals to clinical use. Mitochondrion 7(5):330–339
197. Bird DK, Yan L, Vrotsos KM, Eliceiri KW, Vaughan EM, Keely PJ, White JG, Ramanujam N (2005) Metabolic mapping of MCF10A human breast cells via multiphoton fluorescence lifetime imaging of the coenzyme NADH. Cancer Res 65(19):8766–8773
198. Yu QR, Heikal AA (2009) Two-photon autofluorescence dynamics imaging reveals sensitivity of intracellular NADH concentration and conformation to cell physiology at the single-cell level. J Photochem Photobiol B Biol 95(1):46–57

199. Tadrous PJ, Siegel J, French PMW, Shousha S, Lalani EN, Stamp GW (2003) Fluorescence lifetime imaging of unstained tissues: early results in human breast cancer. J Pathol 199 (3):309–317
200. Provenzano PP, Eliceiri KW, Keely PJ (2009) Multiphoton microscopy and fluorescence lifetime imaging microscopy (FLIM) to monitor metastasis and the tumor microenvironment. Clin Exp Metastasis 26(4):357–370
201. Conklin MW, Provenzano PP, Eliceiri KW, Sullivan R, Keely PJ (2009) Fluorescence lifetime imaging of endogenous fluorophores in histopathology sections reveals differences between normal and tumor epithelium in carcinoma in situ of the breast. Cell Biochem Biophys 53 (3):145–157
202. Skala MC, Riching KM, Gendron-Fitzpatrick A, Eickhoff J, Eliceiri KW, White JG, Ramanujam N (2007) In vivo multiphoton microscopy of NADH and FAD redox states, fluorescence lifetimes, and cellular morphology in precancerous epithelia. Proc Natl Acad Sci U S A 104(49):19494–19499
203. Skala MC, Riching KM, Bird DK, Gendron-Fitzpatrick A, Eickhoff J, Eliceiri KW, Keely PJ, Ramanujam N (2007) In vivo multiphoton fluorescence lifetime imaging of protein-bound and free nicotinamide adenine dinucleotide in normal and precancerous epithelia. J Biomed Opt 12(2)
204. Chorvat D, Chorvatova A (2006) Spectrally resolved time-correlated single photon counting: a novel approach for characterization of endogenous fluorescence in isolated cardiac myocytes. Eur Biophys J Biophys Lett 36(1):73–83
205. Chorvat D, Chorvatova A (2009) Multi-wavelength fluorescence lifetime spectroscopy: a new approach to the study of endogenous fluorescence in living cells and tissues. Laser Phys Lett 6 (3):175–193
206. Wang HW, Gukassyan V, Chen CT, Wei YH, Guo HW, Yu JS, Kao FJ (2008) Differentiation of apoptosis from necrosis by dynamic changes of reduced nicotinamide adenine dinucleotide fluorescence lifetime in live cells. J Biomed Opt 13(5):054011
207. Torno K, Wright BK, Jones MR, Digman MA, Gratton E, Phillips M (2013) Real-time analysis of metabolic activity within lactobacillus acidophilus by phasor fluorescence lifetime imaging microscopy of NADH. Curr Microbiol 66(4):365–367
208. Stringari C, Edwards RA, Pate KT, Waterman ML, Donovan PJ, Gratton E (2012) Metabolic trajectory of cellular differentiation in small intestine by Phasor Fluorescence Lifetime Microscopy of NADH. Sci Rep 2:568
209. Stringari C, Cinquin A, Cinquin O, Digman MA, Donovan PJ, Gratton E (2011) Phasor approach to fluorescence lifetime microscopy distinguishes different metabolic states of germ cells in a live tissue. Proc Natl Acad Sci U S A 108(33):13582–13587
210. Galletly NP, McGinty J, Dunsby C, Teixeira F, Requejo-Isidro J, Munro I, Elson DS, Neil MAA, Chu AC, French PMW, Stamp GW (2008) Fluorescence lifetime imaging distinguishes basal cell carcinoma from surrounding uninvolved skin. Br J Dermatol 159(1):152–161
211. Seidenari S, Arginelli F, Dunsby C, French P, König K, Magnoni C, Manfredini M, Talbot C, Ponti G (2012) Multiphoton laser tomography and fluorescence lifetime imaging of basal cell carcinoma: morphologic features for non-invasive diagnostics. Exp Dermatol 21(11): 831–836
212. Patalay R, Talbot C, Alexandrov Y, Lenz MO, Kumar S, Warren S, Munro I, Neil MAA, König K, French PMW, Chu A, Stamp GWH, Dunsby C (2012) Multiphoton multispectral fluorescence lifetime tomography for the evaluation of basal cell carcinomas. Plos One 7(9): e43460
213. Dancik Y, Favre A, Loy CJ, Zvyagin AV, Roberts MS (2013) Use of multiphoton tomography and fluorescence lifetime imaging to investigate skin pigmentation in vivo. J Biomed Opt 18(2)
214. Sanchez WY, Prow TW, Sanchez WH, Grice JE, Roberts MS (2010) Analysis of the metabolic deterioration of ex vivo skin from ischemic necrosis through the imaging of intracellular NAD (P)H by multiphoton tomography and fluorescence lifetime imaging microscopy. J Biomed Opt 15(4):046008-1–046008-11

215. Sanchez WY, Obispo C, Ryan E, Grice JE, Roberts MS (2012) Changes in the redox state and endogenous fluorescence of in vivo human skin due to intrinsic and photo-aging, measured by multiphoton tomography with fluorescence lifetime imaging. J Biomed Opt 18(6)
216. Arginelli F, Manfredini M, Bassoli S, Dunsby C, French P, König K, Magnoni C, Ponti G, Talbot C, Seidenari S (2013) High resolution diagnosis of common nevi by multiphoton laser tomography and fluorescence lifetime imaging. Skin Res Technol 19(2):194–204
217. Breunig HG, Weinigel M, Buckle R, Kellner-Hofer M, Lademann J, Darvin ME, Sterry W, König K (2013) Clinical coherent anti-Stokes Raman scattering and multiphoton tomography of human skin with a femtosecond laser and photonic crystal fiber. Laser Phys Lett 10(2)
218. Lin LL, Grice JE, Butler MK, Zvyagin AV, Becker W, Robertson TA, Soyer HP, Roberts MS, Prow TW (2011) Time-correlated single photon counting for simultaneous monitoring of zinc oxide nanoparticles and NAD(P)H in intact and barrier-disrupted volunteer skin. Pharm Res 28 (11):2920–2930
219. Schweitzer D, Schenke S, Hammer M, Schweitzer F, Jentsch S, Birckner E, Becker W, Bergmann A (2007) Towards metabolic mapping of the human retina. Microsc Res Tech 70 (5):410–419
220. Schweitzer D, Hammer M, Schweitzer F, Anders R, Doebbecke T, Schenke S, Gaillard ER, Gaillard ER (2004) In vivo measurement of time-resolved autofluorescence at the human fundus. J Biomed Opt 9(6):1214–1222
221. König K, Schneckenburger H, Hibst R (1999) Time-gated in vivo autofluorescence imaging of dental caries. Cell Mol Biol 45(2):233–239
222. Siegel J, Elson DS, Webb SED, Lee KCB, Vlandas A, Gambaruto GL, Lévêque-Fort S, Lever MJ, Tadrous PJ, Stamp GWH (2003) Studying biological tissue with fluorescence lifetime imaging: microscopy, endoscopy, and complex decay profiles. Appl Optics 42(16):2995–3004
223. McConnell G, Girkin JM, Ameer-Beg SM, Barber PR, Vojnovic B, Ng T, Banerjee A, Watson TF, Cook RJ (2007) Time-correlated single-photon counting fluorescence lifetime confocal imaging of decayed and sound dental structures with a white-light supercontinuum source. J Microsc Oxf 225(2):126–136
224. Requejo-Isidro J, McGinty J, Munro I, Elson DS, Galletly NP, Lever MJ, Neil MAA, Stamp GWH, French PMW, Kellett PA, Hares JD, Dymoke-Bradshaw AKL (2004) High-speed wide-field time-gated endoscopic fluorescence-lifetime imaging. Opt Lett 29(19):2249–2251
225. Fruhwirth GO, Ameer-Beg S, Cook R, Watson T, Ng T, Festy F (2010) Fluorescence lifetime endoscopy using TCSPC for the measurement of FRET in live cells. Opt Express 18 (11):11148–11158
226. Sun YH, Hatami N, Yee M, Phipps J, Elson DS, Gorin F, Schrot RJ, Marcu L (2010) Fluorescence lifetime imaging microscopy for brain tumor image-guided surgery. J Biomed Opt 15(5):056022
227. Zeng Y, Wu Y, Li D, Zheng W, Wang WX, Qu JNY (2012) Two-photon excitation chlorophyll fluorescence lifetime imaging: a rapid and noninvasive method for in vivo assessment of cadmium toxicity in a marine diatom *Thalassiosira weissflogii*. Planta 236(5):1653–1663
228. Murata S, Herman P, Lakowicz JR (2001) Texture analysis of fluorescence lifetime images of AT- and GC- rich regions in nuclei. J Histochem Cytochem 49(11):1443–1451
229. Murata S, Herman P, Lakowicz JR (2001) Texture analysis of fluorescence lifetime images of nuclear DNA with effect of fluorescence resonance energy transfer. Cytometry 43(2):94–100
230. Murata S, Herman P, Lin HJ, Lakowicz JR (2000) Fluorescence lifetime imaging of nuclear DNA: effect of fluorescence resonance energy transfer. Cytometry 41(3):178–185
231. van Zandvoort M, de Grauw CJ, Gerritsen HC, Broers JLV, Egbrink M, Ramaekers FCS, Slaaf DW (2002) Discrimination of DNA and RNA in cells by a vital fluorescent probe: lifetime imaging of SYTO13 in healthy and apoptotic cells. Cytometry 47(4):226–235
232. Bacskai BJ, Skoch J, Hickey GA, Allen R, Hyman BT (2003) Fluorescence resonance energy transfer determinations using multiphoton fluorescence lifetime imaging microscopy to characterize amyloid-beta plaques. J Biomed Opt 8(3):368–375

233. Berezovska O, Ramdya P, Skoch J, Wolfe MS, Bacskai BJ, Hyman BT (2003) Amyloid precursor protein associates with a nicastrin-dependent docking site on the presenilin 1-gamma-secretase complex in cells demonstrated by fluorescence lifetime imaging. J Neurosci 23(11):4560–4566
234. Kaminski-Schierle GS, Bertoncini CW, Chan FTS, van der Goot AT, Schwedler S, Skepper J, Schlachter S, van Ham T, Esposito A, Kumita JR, Nollen EAA, Dobson CM, Kaminski CF (2011) A FRET sensor for non-invasive imaging of amyloid formation in vivo. Chemphyschem 12(3):673–680
235. Gu J, Fu CY, Ng BK, Gulam Razul S, Lim SK (2013) Quantitative diagnosis of cervical neoplasia using fluorescence lifetime imaging on haematoxylin and eosin stained tissue sections. J Biophotonics 7(7):483–491
236. Valeur B (2005) Pulse and phase fluorometries: an objective comparison. In: Hof M, Hutterer R, Fidler V (eds) Fluorescence spectroscopy in biology. Springer, Berlin, pp 30–48
237. Becker W, Bergmann A, Hink MA, Konig K, Benndorf K, Biskup C (2004) Fluorescence lifetime imaging by time-correlated single-photon counting. Microsc Res Tech 63(1):58–66
238. Buurman EP, Sanders R, Draaijer A, Gerritsen HC, van Ween JJF, Houpt PM, Levine YK (1992) Fluorescence lifetime imaging using a confocal laser scanning microscope. Scanning 14:155–159
239. Gerritsen HC, Asselbergs NAH, Agronskaia AV, Van Sark WGJHM (2002) Fluorescence lifetime imaging in scanning microscopes: acquisition speed, photon economy and lifetime resolution. J Microsc 206(3):218–224
240. Krishnan RV, Masuda A, Centonze VE, Herman B (2003) Quantitative imaging of protein-protein interactions by multiphoton fluorescence lifetime imaging microscopy using a streak camera. J Biomed Opt 8(3):362–367
241. Biskup C, Zimmer T, Benndorf K (2004) FRET between cardiac Na^+ channel subunits measured with a confocal microscope and a streak camera. Nat Biotechnol 22(2):220–224
242. Minami T, Hirayama S (1990) High quality fluorescence decay curves and lifetime imaging using an elliptical scan streak camera. J Photochem Photobiol A 53:11–21
243. Booth MJ, Wilson T (2004) Low-cost, frequency-domain, fluorescence lifetime confocal microscopy. J Microsc 214(1):36–42
244. Carlsson K, Liljeborg A (1998) Simultaneous confocal lifetime imaging of multiple fluorophores using the intensity-modulated multiple-wavelength scanning (IMS) technique. J Microsc 191(2):119–127
245. French T, So PTC, Weaver DJ, Coelho-Sampaio T, Gratton E, Voss EW, Carrero J (1997) Two-photon fluorescence lifetime imaging microscopy of macrophage-mediated antigen processing. J Microsc 185:339–353
246. Becker W (2005) Advanced time-correlated single photon counting techniques. Springer series in chemical physics, vol 81. Springer: New York
247. O'Connor DV, Phillips D (1984) Time-correlated single-photon counting. Academic, New York
248. Esposito A, Gerritsen HC, Wouters FS (2007) Optimizing frequency-domain fluorescence lifetime sensing for high-throughput applications: photon economy and acquisition speed. J Opt Soc Am A 24:3261
249. Philip J, Carlsson K (2003) Theoretical investigation of the signal-to-noise ratio in fluorescence lifetime imaging. J Opt Soc Am A 20(2):368–379
250. Gratton E, Breusegem S, Sutin J, Ruan Q, Barry N (2003) Fluorescence lifetime imaging for the two-photon microscope: time-domain and frequency-domain methods. J Biomed Opt 8(3):381–390
251. Birch DJS, Imhof RE (1991) Time-domain fluorescence spectroscopy using time-correlated single photon counting. In: Lakowicz JR (ed) Topics in fluorescence spectroscopy: techniques. Plenum Press, New York
252. Lévêque-Fort S, Papadopoulos DN, Forget S, Balembois F, Georges P (2005) Fluorescence lifetime imaging with a low-repetition-rate passively mode-locked diode-pumped Nd:YVO_4 oscillator. Opt Lett 30:168–170

253. Dunsby C, Lanigan PMP, McGinty J, Elson DS, Requejo-Isidro J, Munro I, Galletly N, McCann F, Treanor B, Önfelt B, Davis DM, Neil MAA, French PMW (2004) An electronically tunable ultrafast laser source applied to fluorescence imaging and fluorescence lifetime imaging microscopy. J Phys D Appl Phys 37:3296–3303
254. Esposito A, Bader AN, Schlachter SC, van den Heuvel DJ, Schierle GSK, Venkitaraman AR, Kaminski CF, Gerritsen HC (2011) Design and application of a confocal microscope for spectrally resolved anisotropy imaging. Opt Express 19(3):2546–2555
255. Michalet X et al (2013) Development of new photon-counting detectors for single-molecule fluorescence microscopy. Philos Trans R Soc B Biol Sci 368(1611):20120035
256. Becker W, Su B, Holub O, Weisshart K (2011) FLIM and FCS detection in laser-scanning microscopes: increased efficiency by GaAsP hybrid detectors. Microsc Res Tech 74 (9):804–811
257. Michalet X, Cheng A, Antelman J, Suyama M, Arisaka K, Weiss S (2008) Hybrid photodetector for single-molecule spectroscopy and microscopy. In: SPIE Proc 6862:68620F
258. Walther KA, Papke B, Sinn MB, Michel K, Kinkhabwala A (2011) Precise measurement of protein interacting fractions with fluorescence lifetime imaging microscopy. Mol Biosyst 7 (2):322–336
259. Haugen GR, Wallin BW, Lytle FE (1979) Optimization of data-acquisition rates in time-correlated single-photon fluorimetry. Rev Sci Instrum 50(1):64–79
260. Wang XF, Periasamy A, Herman B, Coleman DM (1992) Fluorescence lifetime imaging microscopy (FLIM): instrumentation and applications. Crit Rev Anal Chem 23 (5):369–395
261. Wang XF, Uchida T, Coleman DM, Minami S (1991) A 2-dimensional fluorescence lifetime imaging system using a gated image intensifier. Appl Spectrosc 45(3):360–366
262. Dowling K, Hyde SCW, Dainty JC, French PMW, Hares JD (1997) 2-D fluorescence lifetime imaging using a time-gated image intensifier. Opt Commun 135(1–3):27–31
263. Scully AD, Mac Robert AJ, Botchway S, O'Neill P, Parker AW, Ostler RB, Phillips D (1996) Development of a laser-based fluorescence microscope with subnanosecond time resolution. J Fluoresc 6(2):119–125
264. Agronskaia AV, Tertoolen L, Gerritsen HC (2003) High frame rate fluorescence lifetime imaging. J Phys D Appl Phys 36(14):1655–1662
265. Dowling K, Dayel MJ, Lever MJ, French PMW, Hares JD, Dymoke-Bradshaw AKL (1998) Fluorescence lifetime imaging with picosecond resolution for biomedical applications. Opt Lett 23(10):810–812
266. Elson DS, Munro I, Requejo-Isidro J, McGinty J, Dunsby C, Galletly N, Stamp GW, Neil MAA, Lever MJ, Kellett PA, Dymoke-Bradshaw A, Hares J, French PMW (2004) Real-time time-domain fluorescence lifetime imaging including single-shot acquisition with a segmented optical image intensifier. New J Phys 6:180
267. Mitchell AC, Wall JE, Murray JG, Morgan CG (2002) Direct modulation of the effective sensitivity of a CCD detector: a new approach to time-resolved fluorescence imaging. J Microsc 206(3):225–232
268. Mitchell AC, Wall JE, Murray JG, Morgan CG (2002) Measurement of nanosecond time-resolved fluorescence with a directly gated interline CCD camera. J Microsc 206(3):233–238
269. Morgan CG, Mitchell AC, Murray JG (1990) Nanosecond time-resolved fluorescence microscopy: principles and practice. Proc R Microsc Soc 1:463–466
270. Pepperkok R, Squire A, Geley S, Bastiaens PIH (1999) Simultaneous detection of multiple green fluorescent proteins in live cells by fluorescence lifetime imaging microscopy. Curr Biol 9(5):269–272
271. Lakowicz JR, Szmacinski H, Nowaczyk K, Berndt KW, Johnson M (1992) Fluorescence lifetime imaging. Anal Biochem 202(2):316–330
272. Gadella TWJ, Jovin TM, Clegg RM (1993) Fluorescence lifetime imaging microscopy (FLIM) – spatial resolution of structures on the nanosecond timescale. Biophys Chem 48:221–239

273. Ng T, Squire A, Hansra G, Bornancin F, Prevostel C, Hanby A, Harris W, Barnes D, Schmidt S, Mellor H, Bastiaens PI, Parker PJ (1999) Imaging protein kinase C alpha activation in cells. Science 283(5410):2085–2089
274. Squire A, Verveer PJ, Bastiaens PIH (2000) Multiple frequency fluorescence lifetime imaging microscopy. J Microsc 197(2):136–149
275. Schneider PC, Clegg RM (1997) Rapid acquisition analysis and display of fluorescence lifetime-resolved images for real-time applications. Rev Sci Instrum 68(11):4107–4119
276. Mizeret J, Stepinac T, Hansroul M, Studzinski A, van den Bergh H, Wagnieres G (1999) Instrumentation for real-time fluorescence lifetime imaging in endoscopy. Rev Sci Instrum 70 (12):4689–4701
277. Mizeret J, Wagnieres G, Stepinac T, Van Den Bergh H (1997) Endoscopic tissue characterization by frequency-domain fluorescence lifetime imaging (FD-FLIM). Lasers Med Sci 12:209–217
278. Hedstrom J, Sedarus S, Prendergast FG (1988) Measurements of fluorescence lifetimes by use of a hybrid time-correlated and multifrequency phase fluorometer. Biochemistry 27:6203–6208
279. Lee KCB, Siegel J, Webb SED, Lévêque-Fort S, Cole MJ, Jones R, Dowling K, Lever MJ, French PMW (2001) Application of the stretched exponential function to fluorescence lifetime imaging. Biophys J 81(3):1265–1274
280. Kress M, Meier T, Steiner R, Dolp F, Erdmann R, Ortmann U, Rück A (2003) Time-resolved microspectrofluorometry and fluorescence lifetime imaging of photosensitizers using picosecond pulsed diode lasers in laser scanning microscopes. J Biomed Opt 8(1):26–32
281. Elson DS, Siegel J, Webb SED, Lévêque-Fort S, Lever MJ, French PMW, Lauritsen K, Wahl M, Erdmann R (2002) Fluorescence lifetime system for microscopy and multi-well plate imaging with a blue picosecond diode laser. Opt Lett 27(16):1409–1411
282. Ryder AG, Glynn TJ, Przyjalgowski M, Szczupak B (2002) A compact violet diode laser-based fluorescence lifetime microscope. J Fluoresc 12(2):177–180
283. Sakai Y, Hirayama S (1988) A fast deconvolution method to analyze fluorescence decays when the excitation pulse repetition period is less than the decay times. J Luminescence 39(3):145–151
284. van Munster EB, Gadella TWJ (2004) phi-FLIM: a new method to avoid aliasing in frequency-domain fluorescence lifetime imaging microscopy. J Microsc 213(1):29–38
285. van Munster EB, Gadella TWJ (2004) Suppression of photobleaching-induced artifacts in frequency-domain FLIM by permutation of the recording order. Cytometry A 58(2):185–194
286. Schuermann KC, Grecco HE (2012) flatFLIM: enhancing the dynamic range of frequency domain FLIM. Opt Express 20(18):20730–20741
287. Becker W, Bergmann A, Biskup C, Zimmer T, Klöcker N, Benndorf K (2002) Multi-wavelength TCSPC lifetime imaging (Invited Paper) [4620–19]. In: SPIE Proc: 4620:79–84
288. Tinnefeld P, Herten DP, Sauer M (2001) Photophysical dynamics of single molecules studied by spectrally-resolved fluorescence lifetime imaging microscopy (SFLIM). J Phys Chem A 105(34):7989–8003
289. Hanley QS, Arndt-Jovin DJ, Jovin TM (2002) Spectrally resolved fluorescence lifetime imaging microscopy. Appl Spectrosc 56(2):155–166
290. Bird DK, Eliceiri KW, Fan CH, White JG (2004) Simultaneous two-photon spectral and lifetime fluorescence microscopy. Appl Optics 43:5173–5182
291. Levitt JA, Matthews DR, Ameer-Beg SM, Suhling K (2009) Fluorescence lifetime and polarization-resolved imaging in cell biology. Curr Opin Biotechnol 20:28–36
292. Jameson DM, Ross JA (2010) Fluorescence polarization/anisotropy in diagnostics and imaging. Chem Rev 110(5):2685–2708
293. Gradinaru CC, Marushchak DO, Samim M, Krull UJ (2010) Fluorescence anisotropy: from single molecules to live cells. Analyst 135(3):452–459
294. Yengo CM, Berger CL (2010) Fluorescence anisotropy and resonance energy transfer: powerful tools for measuring real time protein dynamics in a physiological environment. Curr Opin Pharmacol 10(6):731–737

295. Chan FTS, Kaminski CF, Schierle GSK (2011) HomoFRET fluorescence anisotropy imaging as a tool to study molecular self-assembly in live cells. Chemphyschem 12(3):500–509
296. Vogel SS, Thaler C, Blank PS, Koushik SV (2010) Time-resolved fluorescence anisotropy. In: Ammasi Periasamy RMC (ed) FLIM microscopy in biology and medicine. Chapman & Hall/ Taylor & Francis Group, Boca Raton, pp 245–288
297. Tramier M, Coppey-Moisan M (2008) Fluorescence anisotropy imaging microscopy for homo-FRET in living cells. In: Kevin FS (ed) Methods in cell biology. Academic, Amsterdam, pp 395–414
298. Birch DJS (2011) Fluorescence detections and directions. Meas Sci Technol 22(5):052002
299. Piston DW (2010) Fluorescence anisotropy of protein complexes in living cells. Biophys J 99 (6):1685–1686
300. Axelrod D (1979) Carbocyanine dye orientation in red cell membrane studied by microscopic fluorescence polarization. Biophys J 26(3):557–573
301. Ha T, Laurence TA, Chemla DS, Weiss S (1999) Polarization spectroscopy of single fluorescent molecules. J Phys Chem B 103(33):6839–6850
302. Yan YL, Marriott G (2003) Fluorescence resonance energy transfer imaging microscopy and fluorescence polarization imaging microscopy. Methods in Enzymology, Biophotonics Pt A 360:561–580
303. Fisz JJ (2009) Another treatment of fluorescence polarization microspectroscopy and imaging. J Phys Chem A 113(15):3505–3516
304. Fisz JJ (2007) Another look at magic-angle-detected fluorescence and emission anisotropy decays in fluorescence microscopy. J Phys Chem A 111(50):12867–12870
305. Fisz JJ (2007) Fluorescence polarization spectroscopy at combined high-aperture excitation and detection: application to one-photon-excitation fluorescence microscopy. J Phys Chem A 111(35):8606–8621
306. Koshioka M, Sasaki K, Masuhara H (1995) Time-dependent fluorescence depolarization analysis in 3-dimensional microspectroscopy. Appl Spectrosc 49(2):224–228
307. Fixler D, Namer Y, Yishay Y, Deutsch M (2006) Influence of fluorescence anisotropy on fluorescence intensity and lifetime measurement: theory, simulations and experiments. IEEE Trans Biomed Eng 53(6):1141–1152
308. Axelrod D (1989) Fluorescence polarization microscopy. Methods Cell Biol 30:333–352
309. Suhling K, Siegel J, Lanigan PMP, Leveque-Fort S, Webb SED, Phillips D, Davis DM, French PMW (2004) Time-resolved fluorescence anisotropy imaging applied to live cells. Opt Lett 29 (6):584–586
310. Birch DJS (2001) Multiphoton excited fluorescence spectroscopy of biomolecular systems. Spectrochim Acta A Mol Biomol Spectrosc 57(11):2313–2336
311. Lidke DS, Nagy P, Barisas BG, Heintzmann R, Post JN, Lidke KA, Clayton AHA, Arndt-Jovin DJ, Jovin TM (2003) Imaging molecular interactions in cells by dynamic and static fluorescence anisotropy (rFLIM and emFRET). Biochem Soc Trans 31(5):1020–1027
312. Dix JA, Verkman AS (1990) Mapping of fluorescence anisotropy in living cells by ratio imaging. Applications to cytoplasmic viscosity. Biophys J 57:231–240
313. Swaminathan R, Hoang CP, Verkman AS (1997) Photobleaching recovery and anisotropy decay of green fluorescent protein GFP-S65T in solution and cells: Cytoplasmic viscosity probed by green fluorescent protein translational and rotational diffusion. Biophys J 72:1900–1907
314. Gough AH, Taylor DL (1993) Fluorescence anisotropy imaging microscopy maps calmodulin-binding during cellular contraction and locomotion. J Cell Biol 121(5):1095–1107
315. Levitt JA, Chung PH, Kuimova MK, Yahioglu G, Wang Y, Qu JL, Suhling K (2011) Fluorescence anisotropy of molecular rotors. Chemphyschem 12(3):662–672
316. Bigelow CE, Conover DL, Foster TH (2003) Confocal fluorescence spectroscopy and anisotropy imaging system. Opt Lett 28(9):695–697
317. Foster TH, Pearson BD, Mitra S, Bigelow CE (2005) Fluorescence anisotropy imaging reveals localization of meso-tetrahydroxyphenyl chlorin in the nuclear envelope. Photochem Photobiol 81(6):1544–1547

318. Bigelow CE, Vishwasrao HD, Frelinger JG, Foster TH (2004) Imaging enzyme activity with polarization-sensitive confocal fluorescence microscopy. J Microsc Oxf 215:24–33
319. Li W, Wang Y, Shao HR, He YH, Ma H (2007) Probing rotation dynamics of biomolecules using polarization based fluorescence microscopy. Microsc Res Tech 70(4):390–395
320. Cao Z, Huang CC, Tan W (2006) Nuclease resistance of telomere-like oligonucleotides monitored in live cells by fluorescence anisotropy imaging. Anal Chem 78:1478–1484
321. Mattheyses AL, Hoppe AD, Axelrod D (2004) Polarized fluorescence resonance energy transfer microscopy. Biophys J 87(4):2787–2797
322. Rizzo MA, Piston DW (2005) High-contrast imaging of fluorescent protein FRET by fluorescence polarization microscopy. Biophys J 88(2):L14–L16
323. Matthews DR, Carlin LM, Ofo E, Barber PR, Vojnovic B, Irving M, Ng T, Ameer-Beg SM (2010) Time-lapse FRET microscopy using fluorescence anisotropy. J Microsc Oxf 237 (1):51–62
324. Mao S, Benninger RKP, Yan YL, Petchprayoon C, Jackson D, Easley CJ, Piston DW, Marriott G (2008) Optical lock-in detection of FRET using synthetic and genetically encoded optical switches. Biophys J 94(11):4515–4524
325. Squire A, Verveer PJ, Rocks O, Bastiaens PI (2004) Red-edge anisotropy microscopy enables dynamic imaging of homo-FRET between green fluorescent proteins in cells. J Struct Biol 147 (1):62–69
326. Keating SM, Wensel TG (1991) Nanosecond fluorescence microscopy. Emission kinetics of fura-2 in single cells. Biophys J 59(1):186–202
327. Spitz JA, Polard V, Maksimenko A, Subra F, Baratti-Elbaz C, Meallet-Renault R, Pansu RB, Tauc P, Auclair C (2007) Assessment of cellular actin dynamics by measurement of fluorescence anisotropy. Anal Biochem 367(1):95–103
328. Tramier M, Kemnitz K, Durieux C, Coppey J, Denjean P, Pansu RB, Coppey-Moisan M (2000) Restrained torsional dynamics of nuclear DNA in living proliferative mammalian cells. Biophys J 78(5):2614–2627
329. Clayton AHA, Hanley QS, Arndt-Jovin DJ, Subramaniam V, Jovin TM (2002) Dynamic fluorescence anisotropy imaging microscopy in the frequency domain (rFLIM). Biophys J 83:1631–1649
330. Botchway SW, Lewis AM, Stubbs CD (2011) Development of fluorophore dynamics imaging as a probe for lipid domains in model vesicles and cell membranes. Eur Biophys J Biophys Lett 40(2):131–141
331. Min MY, Rusakov DA, Kullmann DM (1998) Activation of AMPA, kainate, and metabotropic receptors at hippocampal mossy fiber synapses: role of glutamate diffusion. Neuron 21 (3):561–570
332. Perrais D, Ropert N (2000) Altering the concentration of GABA in the synaptic cleft potentiates miniature IPSCs in rat occipital cortex. Eur J Neurosci 12(1):400–404
333. Savtchenko LP, Sylantyev S, Rusakov DA (2013) Central synapses release a resource-efficient amount of glutamate. Nat Neurosci 16(1):10–16
334. Nielsen TA, DiGregorio DA, Silver RA (2004) Modulation of glutamate mobility reveals the mechanism underlying slow-rising AMPAR EPSCs and the diffusion coefficient in the synaptic cleft. Neuron 42(5):757–771
335. Piet R, Vargova L, Sykova E, Poulain DA, Oliet SHR (2004) Physiological contribution of the astrocytic environment of neurons to intersynaptic crosstalk. Proc Natl Acad Sci U S A 101 (7):2151–2155
336. Savtchenko LP, Rusakov DA (2005) Extracellular diffusivity determines contribution of high- versus low-affinity receptors to neural signaling. Neuroimage 25(1):101–111
337. Kukita F (2000) Solvent effects on squid sodium channels are attributable to movements of a flexible protein structure in gating currents and to hydration in a pore. J Physiol Lond 522 (3):357–373
338. Svoboda K, Tank DW, Denk W (1996) Direct measurement of coupling between dendritic spines and shafts. Science 272(5262):716–719

339. Santamaria F, Wils S, De Schutter E, Augustine GJ (2006) Anomalous diffusion in Purkinje cell dendrites caused by spines. Neuron 52(4):635–648
340. Biess A, Korkotian E, Holcman D (2011) Barriers to diffusion in dendrites and estimation of calcium spread following synaptic inputs. Plos Comput Biol 7(10):e1002182
341. Murakoshi H, Wang H, Yasuda R (2011) Local, persistent activation of Rho GTPases during plasticity of single dendritic spines. Nature 472(7341):100–104
342. Nicholson C, Phillips JM, Gardner-Medwin AR (1979) Diffusion from an iontophoretic point source in the brain – role of tortuosity and volume fraction. Brain Res 169(3):580–584
343. Sykova E, Nicholson C (2008) Diffusion in brain extracellular space. Physiol Rev 88 (4):1277–1340
344. Nicholson C, Tao L (1993) Hindered diffusion of high-molecular-weight compounds in brain extracellular microenvironment measured with integrative optical imaging. Biophys J 65 (6):2277–2290
345. Hrabetova S (2005) Extracellular diffusion is fast and isotropic in the stratum radiatum of hippocampal CA1 region in rat brain slices. Hippocampus 15(4):441–450
346. Xiao FR, Nicholson C, Hrabe J, Hrabetova S (2008) Diffusion of flexible random-coil dextran polymers measured in anisotropic brain extracellular space by integrative optical Imaging. Biophys J 95(3):1382–1392
347. Zheng KY, Scimemi A, Rusakov DA (2008) Receptor actions of synaptically released glutamate: the role of transporters on the scale from nanometers to microns. Biophys J 95(10):4584–4596
348. Thorne RG, Nicholson C (2006) In vivo diffusion analysis with quantum dots and dextrans predicts the width of brain extracellular space. Proc Natl Acad Sci U S A 103(14):5567–5572
349. Magzoub M, Zhang H, Dix JA, Verkman AS (2009) Extracellular space volume measured by two-color pulsed dye infusion with microfiberoptic fluorescence photodetection. Biophys J 96 (6):2382–2390
350. Zhang H, Verkman AS (2010) Microfiberoptic measurement of extracellular space volume in brain and tumor slices based on fluorescent dye partitioning. Biophys J 99(4):1284–1291
351. Reits EAJ, Neefjes JJ (2001) From fixed to FRAP: measuring protein mobility and activity in living cells. Nat Cell Biol 3(6):E145–E147
352. Cui-Wang TT, Hanus C, Cui T, Helton T, Bourne J, Watson D, Harris KM, Ehlers MD (2012) Local zones of endoplasmic reticulum complexity confine cargo in neuronal dendrites. Cell 148(1–2):309–321
353. Benninger RKP, Önfelt B, Neil MAA, Davis DM, French PMW (2005) Fluorescence imaging of two-photon linear dichroism: cholesterol depletion disrupts molecular orientation in cell membranes. Biophys J 88:609–622
354. Reeve JE, Corbett AD, Boczarow I, Wilson T, Bayley H, Anderson HL (2012) Probing the orientational distribution of dyes in membranes through multiphoton microscopy. Biophys J 103(5):907–917
355. Brack AS, Brandmeier BD, Ferguson RE, Criddle S, Dale RE, Irving M (2004) Bifunctional rhodamine probes of myosin regulatory light chain orientation in relaxed skeletal muscle fibers. Biophys J 86(4):2329–2341
356. Mojzisova H, Olesiak J, Zielinski M, Matczyszyn K, Chauvat D, Zyss J (2009) Polarization-sensitive two-photon microscopy study of the organization of liquid-crystalline DNA. Biophys J 97(8):2348–2357
357. Dale RE, Eisinger J, Blumberg WE (1979) The orientational freedom of molecular probes. Biophys J 26:161–194
358. van der Meer BW (2002) Kappa-squared: from nuisance to new sense. J Biotechnol 82 (3):181–196
359. Varma R, Mayor S (1998) GPI-anchored proteins are organized in submicron domains at the cell surface. Nature 394:798–801
360. Sharma P, Varma R, Sarasij RC, Ira GK, Krishnamoorthy G, Rao M, Mayor S (2004) Nanoscale organization of multiple GPI-anchored proteins in living cell membranes. Cell 116(4):577–589

361. Vishwasrao HD, Trifilieff P, Kandel ER (2012) In vivo imaging of the actin polymerization state with two-photon fluorescence anisotropy. Biophys J 102(5):1204–1214
362. van Ham TJ, Esposito A, Kumita JR, Hsu S-TD, Kaminski Schierle GS, Kaminski CF, Dobson CM, Nollen EAA, Bertoncini CW (2010) Towards multiparametric fluorescent imaging of amyloid formation: studies of a YFP model of α-synuclein aggregation. J Mol Biol 395(3): 627–642
363. Steinmeyer R, Harms GS (2009) Fluorescence resonance energy transfer and anisotropy reveals both hetero- and homo-energy transfer in the pleckstrin homology-domain and the parathyroid hormone-receptor. Microsc Res Tech 72(1):12–21
364. Gautier I, Tramier M, Durieux C, Coppey J, Pansu RB, Nicolas JC, Kemnitz K, Coppey-Moisan M (2001) Homo-FRET microscopy in living cells to measure monomer-dimer transition of GFP-tagged proteins. Biophys J 80(6):3000–3008
365. Bader AN, Hofman EG, Voortman J, Henegouwen PMPVE, Gerritsen HC (2009) Homo-FRET imaging enables quantification of protein cluster sizes with subcellular resolution. Biophys J 97(9):2613–2622
366. Bader AN, Hofman EG, Henegouwen PMPVE, Gerritsen HC (2007) Imaging of protein cluster sizes by means of confocal time-gated fluorescence anisotropy microscopy. Opt Express 15(11):6934–6945
367. Bader AN, Hoetzl S, Hofman EG, Voortman J, Henegouwen PMPVE, van Meer G, Gerritsen HC (2011) Homo-FRET imaging as a tool to quantify protein and lipid clustering. Chemphyschem 12(3):475–483
368. Yeow EKL, Clayton AHA (2007) Enumeration of oligomerization states of membrane proteins in living cells by homo-FRET spectroscopy and microscopy: theory and application. Biophys J 92(9):3098–3104
369. Thaler C, Koushik SV, Puhl HL, Blank PS, Vogel SS (2009) Structural rearrangement of CaMKII alpha catalytic domains encodes activation. Proc Natl Acad Sci U S A 106(15): 6369–6374
370. Woolley P, Steinhäuser KG, Epe B (1987) Förster-type energy-transfer – simultaneous forward and reverse transfer between unlike fluorophores. Biophys Chem 26(2–3):367–374
371. Porter GB (1972) Reversible energy-transfer. Theor Chim Acta 24(2–3):265–270
372. Willaert K, Loewenthal R, Sancho J, Froeyen M, Fersht A, Engelborghs Y (1992) Determination of the excited-state lifetimes of the tryptophan residues in barnase, via multifrequency phase fluorometry of tryptophan mutants. Biochemistry 31(3):711–716
373. Jung G, Ma YZ, Prall BS, Fleming GR (2005) Ultrafast fluorescence depolarisation in the yellow fluorescent protein due to its dimerisation. Chemphyschem 6(8):1628–1632
374. Koushik SV, Vogel SS (2008) Energy migration alters the fluorescence lifetime of Cerulean: implications for fluorescence lifetime imaging Forster resonance energy transfer measurements. J Biomed Opt 13(3):031204
375. Gee ML, Lensun L, Smith TA, Scholes CA (2004) Time-resolved evanescent wave-induced fluorescence anisotropy for the determination of molecular conformational changes of proteins at an interface. Eur Biophys J Biophys Lett 33(2):130–139
376. Smith TA, Gee ML, Scholes CA (2005) Time-resolved evanescent wave-induced fluorescence anisotropy measurements. In: Lakowicz CDGJR (ed) Reviews in fluorescence. Springer, New York, pp 245–271
377. Digman MA, Caiolfa VR, Zamai M, Gratton E (2008) The phasor approach to fluorescence lifetime imaging analysis. Biophys J 94(2):L14–L16
378. Barber PR, Ameer-Beg SM, Pathmananthan S, Rowley M, Coolen ACC (2010) A Bayesian method for single molecule, fluorescence burst analysis. Biomed Opt Express 1(4):1148–1158
379. Kröger HW, Schmidt GK, Pailer N (1992) Faint object camera: European contribution to the Hubble Space Telescope. Acta Astronaut 26(11):827–834
380. Mason KO, Breeveld A, Much R, Carter M, Cordova FA, Cropper MS, Fordham J, Huckle H, Ho C, Kawakami H (2001) The XMM-Newton optical/UV monitor telescope. Astron Astrophys 365(1):L36–L44

381. Tarhoni MH, Vigneswara V, Smith M, Anderson S, Wigmore P, Lees JE, Ray DE, Carter WG (2011) Detection, quantification, and microlocalisation of targets of pesticides using microchannel plate autoradiographic imagers. Molecules 16(10):8535–8551
382. Rembold CM, Kendall JM, Campbell AK (1997) Measurement of changes in sarcoplasmic reticulum Ca^{2+} in rat tail artery with targeted apoaequorin delivered by an adenoviral vector. Cell Calcium 21(1):69–79
383. Read PD, Carter MK, Pike CD, Harrison RA, Kent BJ, Swinyard BM, Patchett BE, Redfern RM, Shearer A, Colhoun M (1997) Uses of microchannel plate intensified detectors for imaging applications in the X-ray, EUV and visible wavelength regions. Nucl Instrum Methods A392:359–363
384. Sergent N, Levitt JA, Green M, Suhling K (2010) Rapid wide-field photon counting imaging with microsecond time resolution. Opt Express 18(24):25292–25298
385. Suhling K, Hungerford G, Airey RW, Morgan BL (2001) A position-sensitive photon event counting detector applied to fluorescence imaging of dyes in sol–gel matrices. Meas Sci Technol 12:131–141
386. Sharp NA (1992) Millisecond time resolution with the Kitt Peak photon-counting array. Publ Astron Soc Pac 104:263–269
387. Kemnitz K, Pfeifer L, Ainbund MR (1997) Detector for multichannel spectroscopy and fluorescence lifetime imaging on the picosecond timescale. Nucl Instrum Methods Phys Res A 387(1/2):86–87
388. Michalet X, Colyer RA, Antelman J, Siegmund OHW, Tremsin A, Vallerga JV, Weiss S (2009) Single-quantum dot imaging with a photon counting camera. Curr Pharm Biotechnol 10:543–558
389. Esposito A, Gerritsen HC, Oggier T, Lustenberger F, Wouters FS (2006) Innovating lifetime microscopy: a compact and simple tool for life sciences, screening, and diagnostics. J Biomed Opt 11:034016
390. Zhao QL, Schelen B, Schouten R, van den Oever R, Leenen R, van Kuijk H, Peters I, Polderdijk F, Bosiers J, Raspe M, Jalink K, de Jong JGS, van Geest B, Stoop K, Young IT (2012) Modulated electron-multiplied fluorescence lifetime imaging microscope: all-solid-state camera for fluorescence lifetime imaging. J Biomed Opt 17(12):126020
391. Lange R, Seitz P (2001) Solid-state time-of-flight range camera. IEEE J Quantum Electron 37 (3):390–397
392. Kawahito S, Halin IA, Ushinaga T, Sawada T, Homma M, Maeda Y (2007) A CMOS time-of-flight range image sensor with gates-on-field-oxide structure. IEEE Sens J 7(11–12):1578–1586
393. Oggier T, Lehmann M, Kaufmann R, Schweizer M, Richter M, Metzler P, Lang G, Lustenberger F, Blanc N. (2004) An all-solid-state optical range camera for 3D real-time imaging with sub-centimeter depth resolution (SwissRanger). In: Proc SPIE: 5249, 534–545
394. Rochas A, Gani M, Furrer B, Besse PA, Popovic RS, Ribordy G, Gisin N (2003) Single photon detector fabricated in a complementary metal-oxide-semiconductor high-voltage technology. Rev Sci Instrum 74(7):3263–3270
395. Schwartz DE, Charbon E, Shepard KL (2008) A single-photon avalanche diode array for fluorescence lifetime imaging microscopy. IEEE J Solid State Circuits 43(11):2546–2557
396. Pancheri L, Stoppa D (2009) A SPAD-based Pixel Linear Array for High-Speed Time-Gated Fluorescence Lifetime Imaging. In: 2009 Proceedings of Esscirc IEEE, New York, pp 429–432
397. Blacksberg J, Maruyama Y, Charbon E, Rossman GR (2011) Fast single-photon avalanche diode arrays for laser Raman spectroscopy. Opt Lett 36(18):3672–3674
398. Niclass C, Favi C, Kluter T, Gersbach M, Charbon E (2008) A 128 × 128 single-photon image sensor with column-level 10-Bit time-to-digital converter array. IEEE J Solid State Circuits 43(12):2977–2989
399. Niclass C, Rochas A, Besse PA, Charbon E (2005) Design and characterization of a CMOS 3-D image sensor based on single photon avalanche diodes. IEEE J Solid State Circuits 40(9):1847–1854

400. Richardson J, Walker R, Grant L, Stoppa D, Borghetti F, Charbon E, Gersbach M, Henderson RK (2009) A 32x32 50ps resolution 10 bit time to digital converter array in 130 nm CMOS for time correlated imaging. In: Proceedings of the IEEE 2009 custom integrated circuits conference, New York, pp 77–80
401. Gersbach M, Maruyama Y, Trimananda R, Fishburn MW, Stoppa D, Richardson JA, Walker R, Henderson R, Charbon E (2012) A time-resolved, low-noise single-photon image sensor fabricated in deep-submicron CMOS technology. IEEE J Solid State Circuits 47(6):1394–1407
402. Stoppa D, Borghetti F, Richardson J, Walker R, Grant L, Henderson RK, Gersbach M, Charbon E (2009) A 32x32-pixel array with in-pixel photon counting and arrival time measurement in the analog domain. In: 2009 Proceedings of Esscirc, Athens, pp 205–208
403. Veerappan C, Richardson J, Walker R, Day-Uey L, Fishburn MW, Maruyama Y, Stoppa D, Borghetti F, Gersbach M, Henderson RK, Charbon E (2011) A 160x128 single-photon image sensor with on-pixel 55 ps 10b time-to-digital converter. In: Solid-state circuits conference digest of technical papers (ISSCC), San Francisco, 312–314
404. Field R, Shepard KL (2013) A 100-fps fluorescence lifetime imager in standard 0.13-μm CMOS. In 2013 Symposium on VLSI Circuits. VLSI Circuits (VLSIC): Kyoto
405. Arlt J, Tyndall D, Rae BR, Li DDU, Richardson JA, Henderson RK (2013) A study of pile-up in integrated time-correlated single photon counting systems. Rev Sci Instrum 84(10):103105
406. Pancheri L, Massari N, Stoppa D (2013) SPAD image sensor with analog counting pixel for time-resolved fluorescence detection. IEEE Trans Electron Devices 60(10):3442–3449
407. Dutton N, Grant L, Henderson R (2013) 9.8μm SPAD-based analogue single photon counting pixel with bias controlled sensitivity. In: International image sensor workshop. Snowbird, Utah
408. Antonioli S, Cuccato A, Miari L, Labanca I, Rech I, Ghioni M (2013) Ultra-compact 32-channel system for time-correlated single-photon counting measurements. In: SPIE Proc 8773: 87730D
409. Colyer RA, Scalia G, Rech I, Gulinatti A, Ghioni M, Cova S, Weiss S, Michalet X (2010) High-throughput FCS using an LCOS spatial light modulator and an 8 x 1 SPAD array. Biomed Opt Express 1(5):1408–1431
410. Poland SP, Krstajić N, Coelho S, Tyndall D, Walker RJ, Devauges V, Morton PE, Nicholas NS, Richardson J, Li DD-U, Suhling K, Wells CM, Parsons M, Henderson RK, Ameer-Beg SM (2014) Time-resolved multifocal multiphoton microscope for high speed FRET imaging in vivo. Optics Letters, 39(20):6013–6016
411. Fraser GW, Heslop-Harrison JS, Schwarzacher T, Holland AD, Verhoeve P, Peacock A (2003) Detection of multiple fluorescent labels using superconducting tunnel junction detectors. Rev Sci Instrum 74(9):4140–4144
412. Fraser GW, Heslop-Harrison JS, Schwarzacher T, Verhoeve P, Peacock A, Smith SJ (2006) Optical fluorescence of biological samples using STJs. Nucl Instrum Methods Phys Res A 559 (2):782–784
413. Verhoeve P, Martin D, van Dordrecht A, Verveer J, den Hartog R, Peacock A (2003) 120-pixel array of superconducting tunnel junctions as spectrophotometer for optical astronomy. Nucl Instrum Methods Phys Res A 513(1–2):206–210
414. Stevens MJ, Hadfield RH, Schwall RE, Nam SW, Mirin RP, Gupta JA (2006) Fast lifetime measurements of infrared emitters using a low-jitter superconducting single-photon detector. Appl Phys Lett 89:031109
415. Marsili F, Verma VB, Stern JA, Harrington S, Lita AE, Gerrits T, Vayshenker I, Baek B, Shaw MD, Mirin RP, Nam SW (2013) Detecting single infrared photons with 93% system efficiency. Nat Photonics 7(3):210–214
416. Natarajan CM, Tanner MG, Hadfield RH (2012) Superconducting nanowire single-photon detectors: physics and applications. Supercond Sci Technol 25(6):063001
417. Gemmell NR, McCarthy A, Liu BC, Tanner MG, Dorenbos SD, Zwiller V, Patterson MS, Buller GS, Wilson BC, Hadfield RH (2013) Singlet oxygen luminescence detection with a fiber-coupled superconducting nanowire single-photon detector. Opt Express 21(4):5005–5013